Cited2 Regulates Neocortical Layer II/III Generation and Somatosensory Callosal Projection Neuron Development and Connectivity

The Journal of Neuroscience

http://jneurosci.msubmit.net

JN-RM-4067-15R2

Cited2 Regulates Neocortical Layer II/III Generation and Somatosensory Callosal Projection Neuron Development and Connectivity

Jeffrey Macklis, Harvard University
Ryann Fame, Harvard University
Jessica MacDonald, Harvard University
Sally Dunwoodie, University of New South Wales
Emi Takahashi, Boston Children's Hospital

Commercial Interest:

Cited2 Regulates Neocortical Layer II/III Generation and Somatosensory Callosal Projection Neuron Development and Connectivity

Abbreviated title: *Cited2* regulates callosal projection neuron development

Ryann M. Fame[‡1], Jessica L. MacDonald[‡1,4], Sally L. Dunwoodie[2], Emi Takahashi[3], and Jeffrey D. Macklis[1]* ‡ These authors contributed equally to this work.

* Corresponding author: jeffrey_macklis@harvard.edu

Author Affiliations:

[1]Department of Stem Cell and Regenerative Biology, Center for Brain Science, and Harvard Stem Cell Institute, Harvard University, Cambridge, Massachusetts, 02138, [2]Developmental and Stem Cell Biology Division, Victor Chang Cardiac Research Institute, Darlinghurst, Sydney, New South Wales, Australia, Faculties of Medicine and Science, University of New South Wales, Kensington, Sydney, New South Wales, 2052 Australia, [3]Division of Newborn Medicine, Department of Medicine, Boston Children's Hospital, Harvard Medical School; Fetal-Neonatal Neuroimaging and Developmental Science Center, Boston MA 02115; Athinoula A. Martinos Center for Biomedical Imaging, Charlestown, MA, 02129, [4]Current address: Department of Biology, Syracuse University, Syracuse, New York, 13244.

Number of pages: 50; Number of figures: 8; Number of tables: 0; Number of multimedia and 3d models: 0; Word counts: Abstract – 201, Introduction – 653, Discussion - 1496

Conflict of Interest: The authors declare no competing financial interests.

Acknowledgements:

We thank members of the Macklis lab for thoughtful discussions and input, and Lincoln Pasquina, Ryan Richardson, Ben Noble, and Ioana Florea for technical assistance. We thank Prof. Klaus-Armin Nave (Max Planck Institute of Experimental Medicine, Goettingen, Germany) for generously providing the *NEX-Cre* mice. This work and paper were supported by grants from the N.I.H. (R37 NS41590 and NS093376, with additional infrastructure support by NS45523, NS49553, and NS075672), the Jane and Lee Seidman Fund, the Emily and Robert Perlstein Fund, and the United Sydney Association (to J.D.M); National Science Foundation Graduate Research Fellowship Program (GRFP) fellowship, and National Institutes of Health predoctoral NRSA fellowship F31 NS073163 (to R.M.F); Eunice Shriver Kennedy National Institute of Child Health and Human Development (NIH R01HD078561, R21HD069001) (to E.T.); and National Health and Medical Research Council Senior Research Fellowship (ID1042002) (to S.L.D).

Abstract:

The neocortex contains hundreds to thousands of distinct subtypes of precisely connected neurons, allowing it to perform remarkably complex tasks of high-level cognition. Callosal projection neurons (CPN) connect the cerebral hemispheres via the corpus callosum, integrating cortical information, and playing key roles in associative cognition. CPN are a strikingly diverse set of neuronal subpopulations, and development of this diversity requires precise control by a complex, interactive set of molecular effectors. We have identified that the transcriptional co-regulator *Cited2* regulates and refines two stages of CPN development. *Cited2* is expressed broadly by progenitors in the E15.5 SVZ, during the peak of superficial layer CPN birth, with a progressive post-mitotic refinement in expression, becoming restricted to CPN of somatosensory cortex postnatally. We generated progenitor-stage and post-mitotic forebrain-specific *Cited2* conditional knockout (cKO) mice, using the *Emx1-Cre* and *NEX-Cre* mouse lines, respectively. We demonstrate that *Cited2* functions in progenitors, but is not necessary post-mitotically, to regulate both 1) broad generation of layer II/III CPN, and 2) acquisition of precise area-specific molecular identity and axonal/ dendritic connectivity of somatosensory CPN. This novel CPN subtype- and area-specific control from progenitor action of *Cited2* adds yet another layer of complexity to the multi-stage developmental regulation of neocortical development.

Significance Statement:

This study identifies *Cited2* as a novel subtype- and area-specific control over development of distinct subpopulations within the broad population of callosal projection neurons (CPN), whose axons connect the two cerebral hemispheres via the corpus callosum (CC). Currently, how the remarkable diversity of CPN subtypes is specified, and how they

differentiate to form highly precise and specific circuits, is largely unknown. We identified that *Cited2* functions within SVZ progenitors to both broadly regulate generation of superficial layer CPN throughout the neocortex, and to refine precise area-specific development and connectivity of somatosensory CPN. Gaining insight into molecular development and heterogeneity of CPN will advance understanding of both diverse functions of CPN, and the remarkable range of neurodevelopmental deficits correlated with CPN/CC development.

Introduction:

The neocortex contains hundreds to thousands of distinct neuronal subtypes that enable it to perform remarkably complex tasks. Callosal projection neurons (CPN) are the broad population of commissural neurons whose axons connect the two cerebral hemispheres via the corpus callosum (CC), the largest axonal tract in the mammalian brain. CPN are excitatory pyramidal projection neurons whose cell bodies reside in neocortical layers II/III (~80% in mouse), V (~20%), and a few % in VI (Catapano et al., 2001, Fame et al., 2011, Greig et al., 2013), and play key, diverse roles in complex associative and integrative cognition. CPN are molecularly, morphologically, and functionally diverse between the four primary functional neocortical areas (Lomber et al., 1994, Olivares et al., 2001, Grove and Fukuchi-Shimogori, 2003, Benavides-Piccione et al., 2006, O'Leary et al., 2007). Further, subpopulations of CPN maintain other non-callosal projections to contra- or ipsilateral striatum, primary somatosensory cortex, or frontal areas (Wilson, 1987, Mitchell and Macklis, 2005, Fame et al., 2011). CPN are thus a strikingly heterogeneous set of neuronal subpopulations, requiring precise control over development of their distinct subpopulations by a complex and interactive set of molecular controls.

Currently, how the remarkable diversity of CPN subtypes and connectivity is specified, and how they differentiate to form highly precise and specific circuits, is largely unknown. We previously identified a combinatorially-expressed set of genes that both define CPN as a broad population, and identify novel subpopulations of CPN during development (Molyneaux et al., 2009). *Cited2* encodes a transcriptional co-regulator that is significantly enriched in CPN over other cortical projection neuron subpopulations, with particularly high expression at early stages of CPN development (Molyneaux et al., 2009). CITED2 functions as a transcriptional co-

activator by interacting with CBP/p300 (Bhattacharya et al., 1999, Freedman et al., 2003), or as a transcriptional co-repressor by competing with transcription factors for binding to CBP/p300 (Freedman et al., 2003, Lou et al., 2011). *Cited2* is critical for proper development of multiple systems, including heart, lung, lens, placenta, and blood, in addition to neural tube closure (Bamforth et al., 2001, Barbera et al., 2002, Bamforth et al., 2004, Weninger et al., 2005, Withington et al., 2006, Chen et al., 2008, Xu et al., 2008, Chen et al., 2009, Kranc et al., 2009). Although *Cited2* function has not been investigated in cortical development, in these other systems CITED2 interacts with or regulates transcription factors known to function critically in cortical specification and development, including LHX2 (Glenn and Maurer, 1999), PAX6 (Chen et al., 2008, Chen et al., 2009), and AP2γ (Bamforth et al., 2001).

Here, we demonstrate that *Cited2* regulates and refines two stages of CPN development. *Cited2* is expressed broadly by progenitors of the E15.5 SVZ, during the peak of superficial layer CPN birth, with a progressive post-mitotic refinement in expression to CPN of somatosensory cortex postnatally. We generated progenitor-stage and post-mitotic forebrain-specific *Cited2* conditional null (cKO) mice, using the *Emx1-Cre* and *NEX-Cre* mouse lines, respectively. In progenitor-stage cKO, we identify broad reduction of TBR2-positive progenitors at E15.5 across the neocortex, resulting postnatally in both reduced thickness of superficial layers and a highly area-specific reduction of layer II/III somatosensory neocortical length. Importantly, loss of *Cited2* function does not disrupt the barrel field, resulting instead in an unprecedented misalignment of molecular areal identity between layer II/III and layer IV. Further, we identify area-specific disruption of dendritic complexity and precise axonal connectivity of somatosensory CPN. *Cited2* is not required post-mitotically for these functions even though some processes, like arealization and dendritic arborization, are completed post-mitotically.

Taken together, our results demonstrate that *Cited2* functions differently from previously described mechanisms to regulate two stages of precise CPN development, acting in neocortical progenitors to both broadly regulate generation of superficial layer CPN throughout the neocortex, and in an areally-restricted manner to refine the distinct identity and precise connectivity of somatosensory CPN. This novel subtype- and area-specific control from progenitor action adds yet another layer of complexity to the multi-stage development of the neocortex.

Materials and Methods:

Mice

C57Bl/6 wildtype mice were obtained from Charles River Laboratories (Wilmington, MA, USA) for retrograde labeling, Western blotting, and determining gene expression. *Cited2* conditional floxed mice (C2f) (Preis et al., 2006), *Lmo4* conditional floxed mice (L4f) (Deng et al., 2010), and *NEX-Cre* (Goebbels et al., 2006) were previously described. *Emx1*-Cre mice were generated by (Guo et al., 2000) and obtained from The Jackson Laboratory (Bar Harbor, Maine, USA), strain number 005628. To avoid non-specific cre recombinase activity in oocytes (Hayashi et al., 2003), all conditional knockouts were generated by crossing fl females with fl; cre+ males, and no offspring from fl; cre+ dams were analyzed. The morning of the day of the appearance of the vaginal plug was defined as E0.5. The day of birth was designated P0. All animal procedures were approved by Massachusetts General Hospital and/or Harvard University IACUCs.

In Situ Hybridization and Histology

Postnatal tissue was fixed overnight in 4% paraformaldehyde (PFA)/PBS at 4° C; for flatmount analysis, cortices were flattened and fixed three days in 4% PFA/PBS at 4° C. Fixed tissue was sectioned on a vibrating microtome for *in situ* hybridization. Embryonic tissue was flash frozen in 2-methyl butane, embedded in TBS, and cryosectioned. *In situ* hybridization was performed as previously described (Cederquist et al., 2013). The probes were synthesized as described in previous publications: *Cited2* (Molyneaux, et al. 2009); *Rorβ, ephrinA5* ((Allen Brain Atlas Resources, http://www.brain-map.org)); *EphA7* (Mori, et al. 1995); *Cadh8* (Joshi, et al. 2008).

Immunocytochemistry and Western Blotting

Brains were post-fixed overnight in 4% PFA/PBS at 4°C, then were sectioned on a VT1000S vibrating microtome (Leica Microsystems). Sections were incubated in primary antibody dilutions at 4°C overnight, and appropriate secondary antibodies were selected from the Molecular Probes Alexa series (Invitrogen, Carlsbad, CA). Antigen retrieval methods were required to expose antigens for some of the primary antibodies. Sections were incubated in 0.1M citric acid (pH=6.0) for 10 min. at 95-98°C. Primary antibodies were used as follows: goat anti-LMO4 (Santa Cruz Biotech SC-11122), rat anti-TBR2 (eBioscience 14-4875), rabbit anti-TBR2 (Abcam ab23345), rabbit anti- PAX6 (Millipore Ab2237), goat anti-BHLHB5 (Santa Cruz Biotech SC-6045), goat anti-CUX1 (Santa Cruz Biotech SC-13024), mouse anti-PH3 (Abcam ab14955), rabbit anti-PH3 (Upstate 06-570), mouse anti- βIII Tubulin (TUJ1) (Covance mms-435P), mouse anti-PCNA (Sigma WH0005111M2), rat anti-CTIP2 (Abcam ab18465), rabbit anti-Ki67 (Abcam ab15580), rabbit-anti RORβ (a generous gift from the Stunnenberg lab),

rabbit anti-5HT (Immunostar 20080), mouse anti-MBP (Chemicon MAB387), and rabbit anti-GFP (Invitrogen A-11122). Immunocytochemistry was performed as previously described (Cederquist et al., 2013).

Immunoblotting was performed as previously described (Macdonald et al., 2010). Briefly, neocortical tissue was isolated, and protein homogenates were separated by 4-20% SDS–PAGE, and transferred to nitrocellulose membrane (Bio-Rad Trans-Blot). Membranes were incubated for 12–20 hours at 4 °C in rabbit anti-CITED2 (Abcam ab108345) primary antibody diluted in in 2% milk/TBS, and developed with goat anti-rabbit HRP IgG (BioRad) diluted in 2% milk/TBS, and signals were detected with chemiluminescence (Pierce, Rockford, IL).

Quantification of Neocortical Length and Thickness

All length and thickness measurements were performed with images of matched sagittal 50µm sections using ImageJ to trace the curvature of the neocortical surface. Areas were delineated using the noted marker gene expression. Deep layers (V-VI) were identified as those including cells expressing high levels of CTIP2 and deeper. Superficial layers (II-IV) were identified as those superficial to high level CTIP2 expression. p-values were calculated using the unpaired two-tailed Student's T-Test using GraphPad Prism for Mac (GraphPad Software, San Diego California USA, www.graphpad.com). A robust regression outliers (ROUT) test (Q=0.5%) was performed for all data sets with an N equal to or less than 10 (Motulsky and Brown, 2006). No outliers were discovered.

Golgi Staining and Dendritic Complexity Analysis

P22 mouse brains were immersed in freshly prepared impregnation solution (FD Rapid

GolgiStain kit; FD Neurosciences), and processed according to the protocol provided by the company. Neurons were imaged, and then traced blinded to genotype. Dendritic complexity was quantified using Sholl analysis (Sholl, 1953) employing ImageJ (Rasband, W.S., ImageJ, U. S. National Institutes of Health, Bethesda, Maryland, USA) with the Sholl Analysis Plugin (v1.0) (Ghosh Lab, http://labs.biology.ucsd.edu/ghosh/software/). The following parameters were used for dendrite analysis: step= 10 μm, beginning radius= 20 μm, final radius= 200 μm.

High Angular Resolution Diffusion Imaging (HARDI) and Tractography Reconstruction

Adult (9 week old) mouse brains were perfused and fixed for an additional week in 4% paraformaldehyde solution containing 1 mM gadolinium (Gd-DTPA) MRI contrast agent to reduce the T1 relaxation time while ensuring that enough T2 -weighted signal remained. Brains were then scanned on a 4.7T Bruker Biospec MR system. The pulse sequence used for HARDI acquisition was a 3D diffusion-weighted spin-echo echo-planar imaging (EPI) sequence (Tuch et al., 2003) with a spatial resolution of 175 × 175 × 175 μm, sixty diffusion-weighted measurements (high b-value 4,000 sec/mm^2). Diffusion Toolkit and TrackVis (http://trackvis.org) were used to reconstruct and visualize tractography pathways that crossed the midline and passed through both the right and left neocortical hemispheres using an angle threshold of 45°. Tractography was initiated from each voxel within the brain mask, which limits the number of streamlines. Rather than use an FA threshold, brain mask volumes generated from Diffusion Toolkit were used to terminate tractography pathways, because brain abnormalities can result in low FA values that may potentially incorrectly terminate tractography tracing (Takahashi et al., 2010, Rosen et al., 2013, Song et al., 2015). Streamline length was not limited in the analyses. The regions of interest and exclusion were manually drawn from the MRI. We

included all tracts that crossed the midline and passed through both the right and left neocortical hemispheres. Any tract that passed through the anterior commissure was excluded, ensuring that other fiber pathways were not contributing to our analyses.

Anterograde and Retrograde Axonal Labeling

P6 pups were anesthetized by hypothermia, somatosensory neocortex was injected stereotaxically with a pulled glass micropipette (tip diameter 80-100µm), and cell bodies were infected with either AAV-eGFP (Maguire et al., 2013), or the beta subunit of cholera toxin (CTB) labeled with alexa dyes, respectively. Cells were labeled from this boundary area with four tightly clustered injection sites, each consisting of 5 injections of 4.6 nl each at a depth of 250µm. Only brains with matched injections were included in the analysis. Mice were transcardially perfused for analysis at 6 weeks, as outlined previously.

Injection area and contralateral CPN projection spread were analyzed using ImageJ (Rasband, W.S., ImageJ, U. S. National Institutes of Health, Bethesda, Maryland, USA.) Fluorescence intensity was measured in a defined box across the injection in a sagittal section. Total pixels were binned in 100µm bins extending rostrally and caudally from the center of the injection. Fluorescence pixel intensity was calculated as a function of distance from the center of injection within superficial layers of both the injected hemisphere of neocortex and the matched contralateral region. p-values for each bin were calculated using the Bonferroni post-test on the unpaired two-tailed Student's T-Test using GraphPad Prism for Mac. Axonal distribution was divided into 3 regions (anterior tail: -1400µm to -800µm; center: -700µm to 700µm, and posterior tail: 800µm to 1400µm) and two-way ANOVA analysis was performed for each regional distribution using GraphPad Prism for Mac (GraphPad Software, San Diego California

USA, www.graphpad.com). A robust regression outliers (ROUT) test (Q=0.5%) was performed for all data sets with an N equal to or less than 10 (Motulsky and Brown, 2006). No outliers were discovered.

Cell Counts and Density Quantification

E15.5 mouse neocortices were sectioned sagitally, imaged with confocal microscopy at three distinct rostro-caudal positions, and individual cells were quantified based on PAX6-, TBR2-, and PCNA-positivity. Change in basal cell divisions was evaluated by position of pH3-positive mitotic cells. p-values were calculated using the Student's t-test. Neocortical cellular density at P3 was measured in matched sagittal 14 µm cryosections stained for DAPI to mark nuclei, and immunolabeled for LMO4 and CTIP2 to mark areas and laminae. Boxes of standard width were digitally placed over images, and volume was calculated using 14 µm section thickness, measured orthogonal laminar thickness for each sample, and the 280 µm wide box; density is expressed as cells/100 μm^3. p-values were calculated using the unpaired two-tailed Student's t-test. A robust regression outliers (ROUT) test (Q=0.5%) was performed for all data sets with an N equal to or less than 10 (Motulsky and Brown, 2006). No outliers were discovered.

Microscopy and Image Analysis

Tissue sections were imaged on a Nikon 90i microscope using a 1.5 megapixel cooled CCD digital camera (Andor Technology, Dublin, Northern Ireland), or a 5 megapixel color CCD digital camera (Nikon Instruments, Melville, NY). Images were collected and analyzed with

Elements acquisition software (Nikon Instruments, Melville, NY). Laser confocal analysis was performed using a BioRad Radiance 2100 confocal microscope with LaserSharp2000 imaging software (BioRad Laboratories, Hercules, CA). Images were processed using a combination of functions provided by Elements analysis software (Nikon Instruments, Melville, NY), ImageJ (Rasband, W.S., ImageJ, U. S. National Institutes of Health, Bethesda, Maryland, USA), and Adobe Photoshop/ Illustrator software packages (Adobe, San Jose, CA).

Results:

Cited2 is expressed in the SVZ at E15.5 and, postnatally, by a restricted population of somatosensory CPN

The transcriptional co-regulator *Cited2* (CBP/p300-interacting transactivator with glutamic acid (E)/aspartic acid (D)-rich C-terminal domain 2) is more highly expressed by CPN relative to other cortical projection neuron subpopulations (in particular, corticospinal motor neurons, CSMN) in the developing neocortex, with peak differential expression at E18.5, the earliest time point at which CPN and CSMN can be purified by retrograde labeling (Molyneaux et al., 2009) (**Figure 1A**). We confirmed and more broadly investigated the neocortical expression of CITED2 protein by Western blotting from the developing neocortex, revealing high CITED2 expression beginning at E15.5, and decreasing postnatally (**Figure 1B**). *In situ* hybridization reveals that there is minimal pallial expression of *Cited2* at E13.5, but *Cited2* is

highly expressed in progenitor regions throughout the subventricular zone (SVZ) of developing neocortex during superficial layer CPN generation at E15.5 (**Figure 1C,D**), with expression decreasing as differentiation proceeds. Postnatally, total expression levels of *Cited2* decrease, and its neocortical expression strikingly refines to layers II/III, V, and VI of somatosensory areas, mirroring the laminar distribution of CPN (**Figure 1E,F**). To further investigate this refinement of *Cited2* expression, we examined *Cited2* expression in sagittal preparations (**Figure 1G-H**). Embryonically, *Cited2* is expressed across the rostro-caudal extent of the neocortex (**Figure 1G**). Postnatally, *Cited2* expression becomes progressively restricted to CPN (in layers II/III, V, and VI) of somatosensory neocortex by P3, in keeping with the known refinement of molecular areal boundaries (**Figure 1H**). This broad early SVZ progenitor expression across areas, with postnatal areal refinement to somatosensory CPN, led us to hypothesize two stages of function for *Cited2* in neocortical, and specifically CPN, development: broadly in generation of superficial layers, and area-specifically in maturation of somatosensory CPN.

The SVZ is largely composed of intermediate progenitor cells (IPCs; or basal progenitors), which are transit amplifying progenitors that arise from asymmetric divisions of radial glial cells (RGCs) of the VZ, and which undergo a limited number of symmetric divisions before generating pairs of post-mitotic neurons (Haubensak et al., 2004, Miyata et al., 2004, Noctor et al., 2004). Although IPCs give rise to projection neurons of all laminae, at E15.5, the peak of *Cited2* expression, they largely generate superficial layer projection neurons (Sessa et al., 2008, Kowalczyk et al., 2009), of which CPN are the predominant population. The high *Cited2* expression throughout the SVZ suggests a potential *Cited2* function in IPCs at E15.5. At E15.5, *Cited2* is most highly expressed in the laminar domain that overlaps with TBR2-expressing (TBR2+) IPCs of the SVZ, extending into the early post-mitotic neurons of the intermediate

zone, but it is mostly excluded from the region containing PAX6+ RGCs of the VZ (**Figure 1I, J**). The SVZ region expressing *Cited2* includes both proliferating and non-proliferating populations, as assessed by the mitotic markers Ki67 and phosphorylated histone H3 (pH3) (**Figure 1I, K**). Taken together, these data suggest that CITED2 functions in SVZ IPCs as they transition from cycling progenitors to post-mitotic neurons across all areal anlagen at E15.5, when superficial neocortical neurons are being generated.

***Cited2* controls TBR2+ IPC number and proliferation in E15.5 neocortex**

To investigate developmental requirements for *Cited2* in neocortical generation and precise CPN maturation, we generated mice null for *Cited2* in the neocortex. To bypass a set of early patterning defects in homozygous *Cited2* null mutants (Bamforth et al., 2001), and any confounding role *Cited2* might have in the subpallial domain, we generated pallial cortex-specific conditional knockouts using *Emx1*-promoter driven cre-recombinase (*Emx1-Cre*) (Guo et al., 2000, Jin et al., 2000). In all experiments, we compared *Cited2*$^{fl/fl}$; *Emx1-Cre*+ conditional knockout mice (cKO) to littermate controls, both *Cited2*$^{fl/fl}$; *Emx1-Cre*-, and *Cited2*$^{fl/+}$; *Emx1-Cre*+. Because no significant differences were observed between the two control genotypes, they were combined as *Cited2* WT in analyses. We verified that these cKO mutants are viable and healthy, and confirmed that early cortical neurogenesis, preceding onset of pallial *Cited2* expression, is not affected in *Cited2* cKO brains, as assessed by VZ (*Cited2* WT = 2694±36μm, *Cited2* cKO = 2683±56μm; N = 10 WT and 5 cKO, p = 0.87) and cortical plate length (*Cited2* WT = 3163±33μm, *Cited2* cKO = 3093±75μm; p = 0.33) and thickness at E15.5 across the rostro-caudal axis (medial: *Cited2* WT = 317±6μm, *Cited2* cKO = 297±12μm; p = 0.12).

Because *Cited2* is highly expressed throughout the SVZ at E15.5, we specifically investigated whether the population of TBR2+ IPCs is altered in the absence of *Cited2* function. In the setting of a broadly well-patterned and laminated E15.5 neocortex, there is a highly specific ~20% reduction of TBR2+ IPCs in *Cited2* cKO mice **(Figure 2B**), while the number of PAX6+ RGCs is not altered (**Figure 2A**). At this age, only a small fraction of TBR2+ IPCs are actively proliferating, as assessed by PCNA; however, there is a significant decrease in the number of PCNA+ IPCs in *Cited2* cKO mice (**Figure 2C**). The total number of PCNA+ cells, largely PAX6+ RGCs, is not altered in *Cited2* cKO mice (*Cited2* WT = 115±2 PCNA+ cells / 100μm, *Cited2* cKO = 113±2 PCNA+ cells / 100μm; N = 10 WT and 6 cKO, p = 0.67). We directly investigated the population of actively proliferating IPCs as basal mitotic pH3+ progenitors (**Figure 2D**). While there is not a general disruption in mitotic progenitors, there is a specific reduction in basally-located mitotic progenitors, indicating a specific requirement for *Cited2* in IPC proliferation, but not that of RGC.

In addition to perturbed proliferation, a reduction in TBR2+ IPCs might also result from cell death. We directly investigated this possibility by assessing apoptosis at E15.5 using activated caspase 3 (aC3+). We identified a significant increase in aC3+ cells in *Cited2* cKO neocortex, both proliferating progenitors (PCNA+) and post-mitotic neurons (**Figure 2E**). This significant increase in apoptosis among progenitors likely contributes to the substantial decrease in TBR2+ progenitors in *Cited2* cKO neocortex.

The reduction in PCNA+/TBR2+ IPCs and basally-located mitotic progenitors in the *Cited2* cKO neocortex suggests that *Cited2* is necessary for expansion of the IPC population. To directly investigate whether *Cited2* cell-autonomously regulates proliferation of IPCs, we electroporated Cre recombinase into progenitors of $Cited2^{fl/fl}$ and $Cited2^{fl/wt}$ littermates at E14.5,

to excise *Cited2* in a small subpopulation of neocortical progenitors. We co-electroporated GFP to identify progenitors that were cycling at E14.5 and were electroporated, and we employed a BrdU pulse at E15.5 and immunocytochemistry for Ki67 at E16.5 to identify progenitors that continued to proliferate (**Figure 2 F-F'''**). We identified a significant reduction both in the number of *Cited2*-null (*Cited2*$^{fl/fl;}$ Cre+) progenitors that incorporated BrdU at E15.5 and in the number of *Cited2*-null (*Cited2*$^{fl/fl;}$ Cre+) progenitors that were Ki67+ at E16.5. Further, there was a significant reduction in the number of cells proliferating at E15.5 that were still cycling at E16.5 (BrdU/Ki67 double-positive). Additionally, we employed immunocytochemistry for activated caspase 3 (aC3) at E16.5, and did not identify a significant change in the number of *Cited2*-null (*Cited2*$^{fl/fl;}$ Cre+) progenitors that were dying at E16.5. These analyses demonstrate that *Cited2*-null IPCs are less likely to re-enter the cell cycle than their heterozygous counterparts, further supporting the conclusion that *Cited2* cell-autonomously contributes to regulation of IPC proliferation, and that this reduction in basal progenitor proliferation contributes to the reduction in TBR2+ progenitors in *Cited2* cKO neocortex at E15.5.

The later areal refinement of *Cited2* expression raises the hypothesis that CITED2 function in the SVZ is areally restricted based on overlapping, intersectional expression of co-regulators. For example, the known CITED2 interactor AP2γ (Bamforth et al., 2001) is broadly expressed across the ventricular zone; however, it regulates specification of TBR2+ IPCs and generation of superficial layers only in the occipital cortex (Pinto et al., 2009), presumably through an area-restricted co-regulator. To investigate whether *Cited2* functions in an areally-restricted manner within SVZ progenitors, we analyzed IPC numbers in three presumptive areal regions, and determined that the progenitor abnormality is uniform across the extent of the developing neocortex (Tbr2+ cells/100μm: rostral- WT = 76.7 ± 1.6, cKO = 61.7 ± 3.4, p =

0.0004; medial- WT = 69.5 ± 1.9, cKO = 52.2 ± 3.7, p = 0.0003; caudal- WT = 63.7 ± 2.9, cKO = 47.3 ± 5.5, N = 10 WT and 6 cKO, p = 0.01 Student's t-test;), indicating that the function of *Cited2* in IPC proliferation and survival is not areally restricted.

Cited2 regulates neocortical size, including superficial layer thickness and neocortical surface length

Superficial layer CPN arise predominantly from IPCs (Sessa et al., 2008, Kowalczyk et al., 2009); therefore, we investigated whether this significant, broad reduction of IPCs in the *Cited2* null neocortex at E15.5 causes a reduction in superficial layer CPN, presenting as a change either radially in thickness of the superficial layers, and/or tangentially in the cortical length. *Cited2* is not required for gross neocortical development or laminar organization. At postnatal day (P) 6, the *Cited2* cKO neocortex is smaller than WT littermate controls, but both CPN (SATB2+) and CSMN (CTIP2+) are present and appropriately positioned (**Figure 3A**). Anterograde labeling with DiI, and retrograde labeling with fluorescently-conjugated Cholera toxin B (CTB), demonstrate that CPN are present and are appropriately targeting axons to the contralateral hemisphere in *Cited2* cKO neocortex (**Figure 3B, C**). However, both the distribution of retrogradely-labeled CPN (**Figure 3C**), and CUX1 and CTIP2 immunocytochemistry (**Figure 3D**), indicate that superficial layers are reduced in thickness in *Cited2* cKO cortex, while deep layers are not changed in thickness.

Quantitative analysis of neocortical layer thickness at P3 reveals a significant ~20% reduction in superficial layer thickness (layers II/III and IV, as delineated as cells superficial to CTIP2 expression) across multiple neocortical areas, including rostal motor cortex, the primary somatosensory area, and caudal visual cortex. There is no significant change in deep layer

thickness (layer V and VI) in any region, where CPN account for only a minority of projection neurons (**Figure 3E**). To directly investigate whether the reduced superficial layer thickness identified in *Cited2* cKO neocortex is due to reduced cell number and/or increased cell packing, we quantified cell density within the reduced superficial layers. There is no significant difference in cell density in layers II/III of motor or visual cortices, and a modest, but significant, increase in cell density in layer II/III of somatosensory cortex, where the greatest reduction in thickness is observed (motor: *Cited2* WT = 369±128 cells/100μm^3, *Cited2* cKO = 462±30 cells/100μm^3; p = 0.44; somatosensory: *Cited2* WT = 652±66 cells/100μm^3, *Cited2* cKO = 803±26 cells/100μm^3; p = 0.01; visual: *Cited2* WT = 590±35 cells/100μm^3, *Cited2* cKO = =608±7 cells/100μm^3; p = 0.55; N = 6 WT and 3 cKO). Additionally, the reduction in superficial laminar thickness in *Cited2* cKO neocortex persists at P6 (Figure 3D) and into adulthood. These data indicate that the reduction in the number of TBR2+ IPCs observed early in the development of *Cited2* null neocortex results in a significant reduction in the number of superficial layer CPN throughout the neocortex. Interestingly, the findings regarding cell density indicate a further area-specific requirement for *Cited2* in development of layer II/III neurons of somatosensory neocortex.

In addition to the observed reduction in radial thickness in *Cited2* cKO neocortex, early loss of TBR2+ progenitors might also result in an overall decrease in neocortical length on the tangential axis (Sessa et al., 2008, Kowalczyk et al., 2009, Tuoc et al., 2013). We measured cortical surface length at P3, identifying an ~5% smaller diagonal cortical length, and an ~10% reduction in rostro-caudal neocortical surface length in P3 *Cited2* cKO neocortex, measured across multiple medio-lateral sagittal sections (**Figure 3F,G**). These data indicate that there is both significant reduction in cortical thickness as a result of *Cited2* loss of function, and significant reduction in neocortical tangential length. This reduction of cortical length does not

normalize over time; at P21, *Cited2* cKO neocortex is still significantly shorter than that of WT littermates (*Cited2* cKO normalized to *Cited2* WT littermates = 90.9±3% neocortical length; p = 0.005, N = 6 WT and 3 cKO), indicating that the reduction is not simply a delay in maturation, but, rather, a persistent reduction of ~10% of the neocortical rostro-caudal surface length.

Cited2 refines the boundary of areal molecular identity of layer II/III somatosensory CPN

Progressive post-mitotic refinement of *Cited2* expression to somatosensory cortex led us to hypothesize that CITED2 might have a second phase of function in areal-specification of CPN. Dual functions of *Cited2* have previously been identified in eye development, in which *Cited2* acts upstream of *Pax6* to regulate lens morphogenesis, and negatively regulates HIF-1 signaling to regulate hyaloid vasculature formation (Chen et al., 2008). Therefore, we assessed whether specification and development of somatosensory CPN are specifically disrupted in *Cited2* cKO neocortex, beyond the broad reduction in IPCs and superficial layer generation. First, we investigated whether all neocortical areas are uniformly reduced in *Cited2* cKO neocortex, or whether the cortical length reduction is areally restricted.

Strikingly, analysis based on three broad cortical areas distinguished by LMO4 expression at P3 (Joshi et al., 2008) indicates that there is a highly specific and substantial (~35%) reduction in the rostro-caudal length of somatosensory cortex in *Cited2* cKO, versus no significant change in motor or caudal cortex (**Figure 4A-C**). A similar reduction in somatosensory cortex is observed by expression of BHLHB5 (**Figure 5F, H**), which has a largely complementary expression to LMO4, and is highly expressed by CPN of somatosensory neocortex (Joshi et al., 2008, Cederquist et al., 2013). Thus, the entire 10% neocortical tangential

length reduction occurs in the somatosensory region in which *Cited2* is normally expressed postnatally.

Because *Cited2* expression progressively refines to CPN of somatosensory cortex during the first postnatal days, we investigated when the area-specific function of *Cited2* arises. At P0, before motor and somatosensory cortical areas are fully refined, there is a reduction in both motor and somatosensory cortical lengths, as delineated by LMO4 immunostaining (cKO relative length: mot = 0.89 ± 0.04, p = 0.037; SS = 0.83 ± 0.047, p = 0.018; vis = 0.99 ± 0.046, N = 6 WT and 3 cKO, p = 0.89, Student's t-test). The reduction in *Cited2* cKO cortical length progressively becomes restricted to somatosensory cortex by P3 (cKO relative length: mot = 0.94 ± 0.046, p = 0.13; SS = 0.64 ± 0.13, p = 0.0005; vis = 1.02 ± 0.029, N = 8 WT and 4 cKO, p = 0.32, Student's t-test) as wildtype expression of *Cited2* becomes restricted to somatosensory cortex; this specificity for *Cited2* function in somatosensory cortex is maintained at P8 (cKO relative length: SS = 0.73 ± 0.06; N = 10 WT and 5 cKO, $p<0.0001$, Student's t-test).

We confirmed the somatosensory-specific reduction of cortical length in P3 *Cited2* cKO mice using the expression of multiple overlapping and / or complementary molecular markers that, in combination, delineate cortical areas at P3 (Dye et al., 2011). Strikingly, layer II/III measurements of somatosensory cortex length by *Cadh8*, *EphrinA5*, and *EphA7* expression confirm the reduced length observed with Lmo4 measurements (**Figure 4D-F**). Consistent with the CPN subtype-specific expression of *Cited2*, this areal-specific reduction is also layer specific, with no significant difference in length of acallosal layer IV, by expression of *EphrinA5* and *Ror*β in somatosensory cortex in *Cited2* cKO mice (**Figure 4F-G**). In addition, loss of *Cited2* function does not disrupt somatosensory barrel morphology, size, or placement (data not shown).

These results indicate highly specific and significant disruption of layer II/III somatosensory cortex in the absence of *Cited2* function. Taken together, these data suggest that *Cited2* is selectively necessary for acquisition of molecular areal identity of layer II/III somatosensory CPN, but not generally for somatosensory neocortical arealization. In P3 WT neocortex, molecular markers of layer IV primary somatosensory cortex (e.g. Rorβ) and layer II/III somatosensory neocortex (e.g. BHLHB5) align to indicate the boundary between motor and somatosensory cortices (**Figure 4H-H'''**). Notably, upon loss of *Cited2* function, the rostral boundary of Rorβ expression is no longer aligned with BHLHB5 expression, (**Figure 4I-I''')**, but, rather, extends further rostral than the molecularly-identified somatosensory region in layer II/III, indicating an unprecedented misalignment of molecular areal identity between layer II/III and layer IV in the *Cited2* cKO. This neuronal subtype-specific areal misalignment could result in columnar wiring irregularities, the functional consequences of which would be intriguing to investigate in the future.

Cited2 and Lmo4 cooperatively control CPN areal identity

The above evidence indicates functions for *Cited2* in specific acquisition of somatosensory CPN identity, leading to the hypothesis that *Cited2* might act as part of a molecular network to generate neuronal areal identity; additional molecular controls might function in acquisition of other CPN areal identities, interacting with *Cited2* at the boundaries to define these sub-populations. *Lmo4* is a particularly compelling candidate to function in CPN of motor cortex, and to interact with *Cited2* at the motor-somatosensory cortex boundary. *Lmo4* has reciprocal areal expression in the neocortex compared with *Cited2*, and has been shown to have areally-restricted roles in neocortical projection neuron subtype identities and connectivity

(Kashani et al., 2006, Joshi et al., 2008, Lee et al., 2008, Azim et al., 2009, Huang et al., 2009, Cederquist et al., 2013). *Cited2* interacts genetically with *Lmo4*, and *Lmo4* can partially functionally compensate for *Cited2* in thymus development (Michell et al., 2010). This knowledge led us to hypothesize that *Lmo4* might be performing a parallel, areal-specific function in motor cortex CPN, intersecting with *Cited2* in areal boundary regions. Its maintained expression in motor cortex might underlie some of the CPN areal differences observed with *Cited2* loss-of-function.

To test this hypothesis, we generated cortex-specific *Lmo4/Cited2* double conditional knockout (dcKO) mice using *Emx1*-Cre recombinase. While LMO4 plays broader roles in defining neocortical areas and barrel cortex (Kashani et al., 2006, Huang et al., 2009, Cederquist et al., 2013), we focused our analyses on motor and somatosensory superficial layer CPN. Because the *Lmo4* floxed line is maintained on a mixed (C57Bl/6 and S129S6) genetic background, we confirmed that *Cited2* cKO on this background demonstrates the same radial and tangential reductions in neocortical size as identified on a pure C57Bl/6 background. In all analyses, we compared control (*Emx1-Cre* negative), *Lmo4* cKO ($Cited2^{+/+}$;$Lmo4^{fl/fl}$;$Emx1^{Cre/+}$), *Cited2* cKO ($Cited2^{fl/fl}$;$Lmo4^{+/+}$;$Emx1^{Cre/+}$), and double cKO ($Cited2^{fl/fl}$;$Lmo4^{fl/fl}$;$Emx1^{Cre/+}$) littermates.

We identified that the additional loss of *Lmo4* function does not alter the laminar thickness reduction of *Cited2* cKO motor or visual cortex, but does lead to an increase in superficial layer thickness in somatosensory cortex (**Figure 5A-C**). Further, additional loss of *Lmo4* function does not alter the overall tangential neocortical surface length (*Cited2* cKO = 6204 ± 88μm, double cKO = 6453 ± 117 μm; N = 8 Cited2 cKO and 9 double cKO, p = 0.09), as predicted from the post-mitotic restricted expression of LMO4 (Azim et al., 2009, Cederquist et

503 al., 2013). Therefore, *LMO4* and *Cited2* do not genetically interact in the neocortex to control
504 neocortical size. Additionally, mis-expression of *Cited2* does not repress expression of *Lmo4* in
505 motor cortex, nor induce *Lmo4* expression in somatosensory cortex (data not shown). Because
506 *LMO4* is not expressed in neocortical progenitor regions, the maintenance of the reduced
507 neocortical size of *Cited2* cKO cortex in *Lmo4/Cited2* dcKO cortex suggests that the reduction in
508 neocortical size in *Cited2* cKO neocortex results from broad *Cited2* function within the SVZ
509 progenitors.

510 Strikingly, *Lmo4/Cited2* dcKO neocortex, while exhibiting the same reduction in overall
511 length as *Cited2* cKO cortex, has the same somatosensory cortex size as control, exhibiting
512 neither reduction in somatosensory length as exhibited by *Cited2* cKO, nor increase in
513 somatosensory length as seen in *Lmo4* cKO (Kashani et al., 2006, Huang et al., 2009) (**Figure**
514 **5D-H, schematized in Figure 5I-L**). Importantly, the shifts in areal boundaries that occur with
515 single and double loss of *Cited2* and *Lmo4* function are restricted to the motor-somatosensory
516 boundary, with the length of the visual cortex remaining the same across all genotypes. In the
517 context of reduced total neocortical length with loss of *Cited2* function, additional loss of *Lmo4*
518 function results in a rostral shift of the motor-somatosensory boundary (to restore somatosensory
519 cortex length), and reduction in motor cortex length. Taken together, these data indicate that
520 *Cited2* and *Lmo4* participate in a network of compensatory and opposing molecular controls over
521 subtype and specific areal identity within superficial layer CPN of somatosensory and motor
522 cortex. Loss of *Lmo4* function can rescue the superficial layer CPN arealization phenotype found
523 in *Emx1-Cre* driven *Cited2* cKO neocortex.

524

525 ***Cited2* is not required post-mitotically for CPN areal identity**

526 Somatosensory-specific postnatal phenotypes of *Cited2*-null CPN might be dependent on
527 progenitor function of *Cited2*, or they could be fully independent phenotypes, indicating a bi-
528 phasic function for *Cited2* during CPN development. To investigate potential post-mitotic
529 requirements for *Cited2* in acquisition of superficial layer CPN areal identity, we generated mice
530 null for *Cited2* in early post-mitotic neocortical pyramidal neurons using *NEX*-promoter driven
531 cre-recombinase (*NEX-Cre*). In this mouse line, Cre recombinase is expressed specifically in
532 post-mitotic pyramidal neurons of the neocortex and is absent from progenitors, interneurons,
533 oligodendroglia, and astrocytes (Goebbels et al., 2006). Using a highly sensitive cre recombinase
534 reporter (adenovirus GFP), Goebbels, et al. (2006) report that a small number of proliferating
535 cortical cells were observed at E15.5, indicating that there is a very small window of time, if any,
536 between cell cycle exit and onset of *NEX-cre* expression. In *Cited2;NEX-cre* cKO mice, there is
537 highly efficient expression of a β-gal reporter across the postnatal neocortex, indicating highly
538 efficient *Cited2* excision (data not shown).

539 We find that post-mitotic loss of *Cited2* function in the neocortex (with *NEX-cre*
540 excision) does not overtly disrupt neocortical development or laminar organization (**Figure 6A**).
541 Further, there is no reduction in neocortical surface length or laminar thickness in *Cited2;NEX-*
542 *cre* cKOs (Figure 6B-C''), indicating that the reduction in superficial layer CPN observed in the
543 postnatal *Cited2; Emx1-cre* cKO results entirely from *Cited2* function in IPCs. We next
544 investigated whether refinement of layer II/III somatosensory areal identity is disrupted
545 following post-mitotic *Cited2* loss-of-function, as it is following *Emx1*-mediated *Cited2* excision.
546 Interestingly, there is no disruption in somatosensory length in P3 *Cited2; NEX-cre* cKO
547 neocortex (**Figure 6D-E**). Taken together, these results indicate that the reduction in acquisition

548 of layer II/III somatosensory areal identity results from *Cited2* function in neocortical
549 progenitors, and it is not a fully independent post-mitotic function of *Cited2*.
550
551 ***Disruption of area-apecific CPN dendritic complexity following excision of Cited2 in***
552 ***progenitors***
553 *Cited2* functions broadly in early IPCs to both regulate generation of neocortical
554 superficial layer CPN broadly, and to control acquisition of somatosensory molecular areal
555 identity by layer II/III somatosensory CPN specifically. Somatosensory CPN have unique
556 connectivity features, both in their afferent and efferent connections (Innocenti and Price, 2005,
557 Benavides-Piccione et al., 2006). We therefore directly investigated potential functions of *Cited2*
558 in central properties of their specific connectivity that govern the unique functionality of
559 somatosensory CPN. We first examined neuronal soma size across all lamina and areas of
560 *Cited2; Emx-cre* cKOs to determine if *Cited2* loss-of-function disrupts overall size or growth of
561 cortical projection neurons. Using NeuN to mark neuronal somata, we found no change in
562 neuronal soma size (average soma cross-sectional area) at P21 in either deep or superficial layers
563 (**Figure 7A**). These results indicate that the reduced superficial layer thickness (**Figure 3**) is not
564 due to decreased CPN soma size.
565 We then investigated dendritic complexity of layer II/III CPN by Golgi staining and Sholl
566 analysis in multiple neocortical areas (**Figure 7**). While there is no significant change in layer
567 II/III CPN dendritic complexity within motor or visual cortex in the *Cited2; Emx1*-cre cKO
568 mice, there is a significant increase in CPN dendritic complexity in somatosensory cortex
569 (**Figure 7B-D**). In *Cited2* WT neocortex, dendritic complexity of layer II/III CPN is distinct
570 across different neocortical areas (**Figure 7E**), with decreasing complexity rostral to caudal, as

has been shown previously (Benavides-Piccione et al., 2006). Interestingly, there is a shift in total dendritic arbor distribution in *Cited2; Emx1-cre* cKO somatosensory cortex CPN to more closely resemble CPN in motor cortex, with more dendrites close to neuronal cell bodies (**Figure 7F**). Taken together these results indicate that dendritic complexity is specifically increased in somatosensory CPN in *Cited2; Emx1*-cre cKO cortex, perhaps suggesting that *Cited2*-null CPN might be partially 'motorized' with respect to dendritic complexity.

Because dendritic arborization occurs post-mitotically, we investigated whether dendritic development of somatosensory CPN is also perturbed following post-mitotic-specific *Cited2* loss-of-function, or whether it is dependent on the reduction in acquisition of layer II/III somatosensory areal identity that results from *Cited2* function in neocortical progenitors. We find that *NEX-cre* mediated excision of *Cited2* does not alter CPN soma size (data not shown) or CPN dendritic complexity in any area (**Figure 7G-I**). Together, these data indicate that continuous post-mitotic expression of *Cited2* in somatosensory CPN is not required for development of areal subpopulation-appropriate CPN size and dendritic complexity; rather, alterations in CPN generation and areal identity acquisition arising from *Cited2* function in progenitors disrupts development of somatosensory-specific CPN dendritic complexity.

***Cited2* is required for precise, homotopic CPN axonal connectivity**

In addition to area-specific dendritic complexity, we investigated potential *Cited2* function in CPN axonal connectivity, both broadly and in an area-specific manner. High-angular resolution diffusion imaging (HARDI) tractography based on magnetic resonance imaging (MRI) reveals that there are fewer correlated pathways passing throughout the corpus callosum (CC) of adult *Cited2* cKO mouse brains as compared to control (**Figure 8A-B**), consistent with

the overall reduction in superficial layer thickness and CPN number. The reduced CC is confirmed by examining myelinated fibers in mid-sagittal sections labeled with myelin basic protein (MBP), revealing a significantly smaller CC area **(Figure 8C-D)**. Overall forebrain and midbrain area is not reduced in *Cited2* cKO mice, as measured on these mid-sagittal sections (WT = 38.6 ± 0.7 μm^2, cKO = 37.0 ± 0.8 μm^2; N = 3 WT, 4 cKO; p = 0.18), and *Cited2* cKO CC area is reduced relative to brain area (p = 0.04). Neocortical area, on the other hand, is reduced in *Cited2* cKO mice (WT = 11.5 ± 0.3 μm^2, cKO = 10.1 ± 0.3 μm^2; N = 3 WT, 4 cKO; p = 0.02), suggesting that the reduced CC area in *Cited2* cKO mice results from the reduced number of CPN. Of particular note, HARDI reveals an apparent additional disruption in callosal fibers in mid-CC, even though the CC is overall present, but reduced, by MBP staining, suggesting localized axonal disorganization in addition to fewer fibers (**Figure 8A',B'**).

We directly investigated precision of CPN projections at the border between motor and somatosensory cortical areas, which is especially molecularly disrupted in *Cited2; Emx1* cKO mouse cortex during development. Precisely matched, focal AAV-GFP anterograde labeling demonstrates that *Cited2; Emx1* cKO somatosensory CPN project contralateral axons imprecisely, with a bimodal distribution of axonal projections covering a more expansive target area on the contralateral hemisphere than the tightly delineated homotopic areas targeted by WT CPN (**Figures 8E-K)**. Taken together, these data indicate that *Cited2* is required for precise areal-specific connectivity of somatosensory CPN, both afferent and efferent.

Discussion:

CPN are a remarkably diverse set of neuronal subpopulations, requiring precise control over development of these subpopulations for proper organization and function. This study demonstrates that the transcriptional co-regulator CITED2 regulates two aspects of precise CPN development in mouse. *Cited2* functions broadly in embryonic progenitors of the SVZ to regulate generation of superficial layer CPN throughout the neocortex. *Cited2* also functions within progenitors to establish the distinct identity and development of somatosensory CPN, in an areally restricted manner. Understanding molecular controls over development of CPN subpopulations, such as CITED2 control over somatosensory layer II/III CPN, will advance understanding of diverse system functions of CPN, and the broad range of neurodevelopmental disorders with associated abnormalities of CPN / corpus callosum development – both overt and subtle.

***Cited2* regulates the precise number of TBR2+ IPCs generating layer II/III CPN**

The SVZ has expanded concomitantly with the expansion of the cerebral cortex during mammalian evolution, suggesting that an increase in IPCs contributes substantially to the evolutionary expansion of the neocortex (Kriegstein et al., 2006, Martinez-Cerdeno et al., 2006, Molnar et al., 2006, Noctor et al., 2008, Betizeau et al., 2013). Disrupting the IPC population results in reduced cortical thickness of all layers, and reduced cortical surface area (Sessa et al., 2008, Kowalczyk et al., 2009, Tuoc et al., 2013), with superficial layers most significantly impacted (Pontious et al., 2008). Expression of *Cited2* in the SVZ peaks during generation of superficial layers, and loss of *Cited2* function disrupts generation of superficial layers specifically. CUX2 similarly is expressed by IPCs only during late neurogenesis, and its loss

636 perturbs superficial layer neuron production specifically (Cubelos et al., 2008), further
637 highlighting the increased molecular regulation, in which *Cited2* has a substantial role,
638 controlling the production of this set of neuronal populations.

639 The reduction in *Cited2; Emx1-cre* cKO neocortical superficial layers arises from a
640 significant reduction of TBR2+ IPCs at E15.5, the peak of superficial layer neuron birth. This
641 reduction in TBR2+ IPCs likely results from both an increase in basal progenitor death, and a
642 decrease in IPC proliferation /cell cycle re-entry. We identified an approximately 2-fold increase
643 in cell death in *Cited2* cKO neocortex, including both progenitors and post-mitotic cells.
644 Increased apoptosis is also evident in the midbrain of *Cited2*-/- embryos during neural tube
645 closure (Bamforth et al., 2001, Barbera et al., 2002), and CITED2 regulates death of cortical
646 neurons *in vitro* after induced DNA damage (Gonzalez et al., 2008).

647 In addition to increased apoptosis, there is a significant reduction in the number of
648 proliferating IPCs at E15.5, and cell-autonomous *Cited2* loss-of-function results in reduced cell
649 cycle re-entry between E14.5 and E16.5, suggesting that *Cited2* function is required to maintain
650 and expand these transit-amplifying progenitors. In line with this interpretation, *Cited2* is highly
651 up-regulated by actively proliferating transit amplifying progenitors during induced regeneration
652 in the olfactory epithelium (Shetty et al., 2005). Further, CITED2 controls proliferation in
653 fibroblasts (Kranc et al., 2003), hematopoietic stem cells (Du and Yang, 2013), and non-small-
654 cell lung cancer cells (Chou et al., 2012). Taken together, the reduction in TBR2+ IPCs in E15.5
655 *Cited2* cKO SVZ is likely due, at least in large part, to reduced proliferation within this
656 progenitor population, in addition to the identified apoptosis increase.

657

658 ***Cited2* functions in concert with distinct transcriptional regulators**

Transcription factors that play roles in both areal and laminar identity have been identified. For example, TBR1 functions in post-mitotic neurons to regulate the appropriate differentiation of layer VI broadly, as well as the establishment of frontal cortex identity (Hevner et al., 2001, Bedogni et al., 2010), and PAX6 functions in progenitor cells to both regulate neurogenesis and promote rostral identity (Bishop et al., 2002, Schuurmans et al., 2004). The dual functions of *Cited2* in CPN development appear to be quite different from these previously described mechanisms, however. *Cited2* functions broadly in SVZ progenitors to regulate the generation of (primarily) layer II/III neurons; *Cited2* also has a progenitor function leading to the acquisition of appropriate areal identity of a subpopulation of superficial layer CPN. Unlike areal identity genes, such as PAX6, Bhlhb5, and TBR1 (Joshi et al., 2008, Bedogni et al., 2010), loss of *Cited2* function does not disrupt establishment of areal identity, *per se*. This is demonstrated by the apparently normal development of the barrel field, the hallmark of the primary somatosensory cortex, in the context of an areal disruption in somatosensory layer II/III. These results strongly suggest that CITED2 functions as part of a complex network of transcriptional co-regulators that interact, compete, and compensate to regulate and refine appropriate acquisition of areal identity within a particular projection neuron subpopulation, layer II/III CPN of somatosensory cortex.

We hypothesized that the transcriptional co-regulator LMO4 might function as part of this network, regulating the acquisition of areal identity of layer II/III CPN of motor cortex. We identified that additional removal of *Lmo4* from *Cited2* cKO neocortex results in a balanced reduction of molecularly defined motor and somatosensory areas within layer II/III, compared to the specific reduction in layer II/III somatosensory area with loss of *Cited2* alone, and increase in layer II/III somatosensory area with loss of *Lmo4* alone. Loss of *Cited2* and *Lmo4* function,

682 alone and in combination, does not result in complete loss of areal identity; rather, areal
683 boundaries shift, highlighting that these transcriptional co-regulators provide a mutually
684 dependent and partially antagonistic level of precise regulation of neuronal subtype-specific areal
685 identity acquisition.
686
687 **Precise connectivity of somatosensory CPN**
688 Laminar composition and circuit organization is distinct within the primary
689 somatosensory neocortex compared with other neocortical areas (Polleux et al., 2001, Rash and
690 Grove, 2006, Dehay and Kennedy, 2007, O'Leary et al., 2007). The unique misalignment of layer
691 II/III somatosensory neocortex relative to layer IV barrel cortex in *Cited2* cKO neocortex likely
692 profoundly perturbs this precise circuitry, as evidenced, in part, by the disrupted dendritic
693 complexity and precise axonal connectivity of *Cited2* cKO CPN. Dendritic complexity of layer
694 II/III CPN is specific to each neocortical area in mice, with dendritic arbors becoming
695 progressively more complex from caudal to rostral areas (Benavides-Piccione et al., 2006). CPN
696 of *Cited2*-null somatosensory cortex display increased dendritic complexity that highly
697 resembles that normally found in CPN of motor cortex. This is despite the fact that CPN from the
698 motor / somatosensory border regions, where molecular boundaries are shifted during
699 development**,** were excluded from this analysis. Layer II/III CPN that are within the molecularly
700 defined somatosensory cortex (i.e. BHLHB5+/LMO4-) of *Cited2* cKO mice develop dendritic
701 morphology of CPN of normal motor cortex, indicating critical roles for *Cited2* in somatosensory
702 CPN afferent connectivity.
703 Within young adult *Cited2* cKO neocortex, CPN projections from the disrupted motor /
704 somatosensory region are also quite imprecise, demonstrating a bimodal distribution of

projections rostro-caudally within somatosensory cortex. Further, high-angular resolution diffusion imaging (HARDI) identifies reduced callosal connectivity, particularly in mid-callosum, correlating with somatosensory cortex. Normally, ectopic CPN projections are eliminated through activity-dependent mechanisms over the first postnatal weeks (Innocenti and Price, 2005, Luo and O'Leary, 2005, Mizuno et al., 2007, Wang et al., 2007, Zhou et al., 2013). The atypical projections identified in adult *Cited2* cKO neocortex might be aberrantly maintained, and might indicate earlier disrupted neuronal activity of *Cited2*-null CPN during somatosensory cortex development. It has recently been shown that balanced thalamic input regulates targeting of callosal projections in somatosensory cortex (Suarez et al., 2014). Even though post-mitotic loss of *Cited2* does not disrupt the metrics assessed here in somatosensory CPN, it would be of interest in future studies to assess whether *Cited2* might be induced or maintained in post-mitotic somatosensory CPN in response to such balanced activity, leading to specific acquisition of other somatosensory CPN features.

In humans, even subtle disruptions in callosal connectivity are associated with defects in abstract reasoning, problem solving, and generalization (Paul et al., 2007), as well as with multiple neurodevelopmental disorders, including autism spectrum disorders (ASD) (Egaas et al., 1995, Piven et al., 1997, Herbert and Kenet, 2007, Frazier and Hardan, 2009, Hardan et al., 2009), attention deficit hyperactivity disorder (Hynd et al., 1991, Roessner et al., 2004, Seidman et al., 2005), Tourette's syndrome (Plessen et al., 2006), and schizophrenia (Swayze et al., 1990, Tibbo et al., 1998, Innocenti et al., 2003, Wolf et al., 2008). Further, perturbed dendritic complexity of layer II/III CPN is observed in multiple neurodevelopmental disorders, including Rett syndrome (Armstrong et al., 1995, Kishi and Macklis, 2004), ASD (Mukaetova-Ladinska et al., 2004, Srivastava et al., 2012), and schizophrenia (Broadbelt et al., 2002). Greater

understanding of molecular regulation of precise temporal and area-specific development of diverse CPN subpopulations might elucidate perturbations underlying such complex neurodevelopmental disorders.

Conclusions

Taken together, our results demonstrate that *Cited2* functions differently from previously described mechanisms to regulate two stages of precise CPN development, acting in neocortical progenitors to both broadly regulate generation of superficial layer CPN throughout the neocortex, and in an areally-restricted manner to refine the distinct identity and precise connectivity of somatosensory CPN. This novel biology of *Cited2* adds yet another layer of complexity to the multi-stage control and regulation of neocortical development.

Author Contributions

R.M.F, J.L.M, and J.D.M. designed the experiments. R.M.F. and J.L.M. performed all of the experiments, except the DSI/HARDI imaging; E.T. performed imaging for the DSI/HARDI experiments. S.L.D. provided *Cited2* mouse lines and developed specialized genotyping protocols. R.M.F, J.L.M, and J.D.M. wrote the manuscript, with input from E.T. and S.L.D.

References:

Armstrong D, Dunn JK, Antalffy B, Trivedi R (1995) Selective dendritic alterations in the cortex of Rett syndrome. J Neuropathol Exp Neurol 54:195-201.

Azim E, Shnider SJ, Cederquist GY, Sohur US, Macklis JD (2009) Lmo4 and Clim1 progressively delineate cortical projection neuron subtypes during development. Cereb Cortex 19 Suppl 1:i62-69.

Bamforth SD, Bragança J, Eloranta JJ, Murdoch JN, Marques FI, Kranc KR, Farza H, Henderson DJ, Hurst HC, Bhattacharya S (2001) Cardiac malformations, adrenal agenesis, neural crest defects and exencephaly in mice lacking Cited2, a new Tfap2 co-activator. Nat Genet 29:469-474.

Bamforth SD, Bragança J, Farthing CR, Schneider JE, Broadbent C, Michell AC, Clarke K, Neubauer S, Norris D, Brown NA, Anderson RH, Bhattacharya S (2004) Cited2 controls left-right patterning and heart development through a Nodal-Pitx2c pathway. Nat Genet 36:1189-1196.

Barbera JP, Rodriguez TA, Greene ND, Weninger WJ, Simeone A, Copp AJ, Beddington RS, Dunwoodie S (2002) Folic acid prevents exencephaly in Cited2 deficient mice: Creation of CITED2 null mice. Hum Mol Genet 11:283-293.

Bedogni F, Hodge RD, Elsen GE, Nelson BR, Daza RA, Beyer RP, Bammler TK, Rubenstein JL, Hevner RF (2010) Tbr1 regulates regional and laminar identity of postmitotic neurons in developing neocortex. Proc Natl Acad Sci U S A 107:13129-13134.

Benavides-Piccione R, Hamzei-Sichani F, Ballesteros-Yanez I, DeFelipe J, Yuste R (2006) Dendritic size of pyramidal neurons differs among mouse cortical regions. Cereb Cortex 16:990-1001.

768 Betizeau M, Cortay V, Patti D, Pfister S, Gautier E, Bellemin-Menard A, Afanassieff M,
769 Huissoud C, Douglas RJ, Kennedy H, Dehay C (2013) Precursor diversity and
770 complexity of lineage relationships in the outer subventricular zone of the primate.
771 Neuron 80:442-457.
772 Bhattacharya S, Michels CL, Leung MK, Arany ZP, Kung AL, Livingston DM (1999)
773 Functional role of p35srj, a novel p300/CBP binding protein, during transactivation by
774 HIF-1. Genes Dev 13:64-75.
775 Bishop KM, Rubenstein JL, O'Leary DD (2002) Distinct actions of Emx1, Emx2, and Pax6 in
776 regulating the specification of areas in the developing neocortex. J Neurosci 22:7627-
777 7638.
778 Broadbelt K, Byne W, Jones LB (2002) Evidence for a decrease in basilar dendrites of pyramidal
779 cells in schizophrenic medial prefrontal cortex. Schizophr Res 58:75-81.
780 Catapano LA, Arnold MW, Perez FA, Macklis JD (2001) Specific neurotrophic factors support
781 the survival of cortical projection neurons at distinct stages of development. J Neurosci
782 21:8863-8872.
783 Cederquist GY, Azim E, Shnider SJ, Padmanabhan H, Macklis JD (2013) Lmo4 establishes
784 rostral motor cortex projection neuron subtype diversity. J Neurosci 33:6321-6332.
785 Chen Y, Carlson EC, Chen ZY, Hamik A, Jain MK, Dunwoodie SL, Yang YC (2009)
786 Conditional deletion of Cited2 results in defective corneal epithelial morphogenesis and
787 maintenance. Dev Biol 334:243-252.
788 Chen Y, Doughman Y-Q, Gu S, Jarrell A, Aota S-I, Cvekl A, Watanabe M, Dunwoodie SL,
789 Johnson RS, Van Heyningen V, Kleinjan DA, Beebe DC, Yang Y-C (2008) Cited2 is
790 required for the proper formation of the hyaloid vasculature and for lens morphogenesis.
791 Development 135:2939-2948.
792 Chou YT, Hsieh CH, Chiou SH, Hsu CF, Kao YR, Lee CC, Chung CH, Wang YH, Hsu HS,
793 Pang ST, Shieh YS, Wu CW (2012) CITED2 functions as a molecular switch of
794 cytokine-induced proliferation and quiescence. Cell Death Differ 19:2015-2028.
795 Cubelos B, Sebastian-Serrano A, Kim S, Moreno-Ortiz C, Redondo JM, Walsh CA, Nieto M
796 (2008) Cux-2 controls the proliferation of neuronal intermediate precursors of the cortical
797 subventricular zone. Cereb Cortex 18:1758-1770.

798 Dehay C, Kennedy H (2007) Cell-cycle control and cortical development. Nat Rev Neurosci
799 8:438-450.
800 Deng M, Pan L, Xie X, Gan L (2010) Requirement for Lmo4 in the vestibular morphogenesis of
801 mouse inner ear. Dev Biol 338:38-49.
802 Du J, Yang YC (2013) Cited2 in hematopoietic stem cell function. Curr Opin Hematol 20:301-
803 307.
804 Dye CA, El Shawa H, Huffman KJ (2011) A lifespan analysis of intraneocortical connections
805 and gene expression in the mouse I. Cereb Cortex 21:1311-1330.
806 Egaas B, Courchesne E, Saitoh O (1995) Reduced size of corpus callosum in autism. Arch
807 Neurol 52:794-801.
808 Fame RM, MacDonald JL, Macklis JD (2011) Development, specification, and diversity of
809 callosal projection neurons. Trends Neurosci 34:41-50.
810 Frazier TW, Hardan AY (2009) A meta-analysis of the corpus callosum in autism. Biol
811 Psychiatry 66:935-941.
812 Freedman SJ, Sun Z-YJ, Kung AL, France DS, Wagner G, Eck MJ (2003) Structural basis for
813 negative regulation of hypoxia-inducible factor-1alpha by CITED2. Nat Struct Biol
814 10:504-512.
815 Glenn DJ, Maurer RA (1999) MRG1 binds to the LIM domain of Lhx2 and may function as a
816 coactivator to stimulate glycoprotein hormone alpha-subunit gene expression. J Biol
817 Chem 274:36159-36167.
818 Goebbels S, Bormuth I, Bode U, Hermanson O, Schwab MH, Nave KA (2006) Genetic targeting
819 of principal neurons in neocortex and hippocampus of NEX-Cre mice. Genesis 44:611-
820 621.
821 Gonzalez Y, Zhang Y, Behzadpoor D, Cregan S, Bamforth S, Slack R, Park D (2008) CITED2
822 Signals through Peroxisome Proliferator-Activated Receptor- to Regulate Death of
823 Cortical Neurons after DNA Damage. Journal of Neuroscience 28:5559-5569.
824 Greig LC, Woodworth MB, Galazo MJ, Padmanabhan H, Macklis JD (2013) Molecular logic of
825 neocortical projection neuron specification, development and diversity. Nat Rev Neurosci
826 14:755-769.
827 Grove EA, Fukuchi-Shimogori T (2003) Generating the cerebral cortical area map. Annu Rev
828 Neurosci 26:355-380.

829 Guo H, Hong S, Jin XL, Chen RS, Avasthi PP, Tu YT, Ivanco TL, Li Y (2000) Specificity and
830 efficiency of Cre-mediated recombination in Emx1-Cre knock-in mice. Biochem Biophys
831 Res Commun 273:661-665.
832 Hardan AY, Pabalan M, Gupta N, Bansal R, Melhem NM, Fedorov S, Keshavan MS, Minshew
833 NJ (2009) Corpus callosum volume in children with autism. Psychiatry Res 174:57-61.
834 Haubensak W, Attardo A, Denk W, Huttner WB (2004) Neurons arise in the basal
835 neuroepithelium of the early mammalian telencephalon: a major site of neurogenesis.
836 Proc Natl Acad Sci U S A 101:3196-3201.
837 Hayashi S, Tenzen T, McMahon AP (2003) Maternal inheritance of Cre activity in a Sox2Cre
838 deleter strain. Genesis 37:51-53.
839 Herbert MR, Kenet T (2007) Brain abnormalities in language disorders and in autism. Pediatr
840 Clin North Am 54:563-583, vii.
841 Hevner RF, Shi L, Justice N, Hsueh Y, Sheng M, Smiga S, Bulfone A, Goffinet AM,
842 Campagnoni AT, Rubenstein JL (2001) Tbr1 regulates differentiation of the preplate and
843 layer 6. Neuron 29:353-366.
844 Huang Z, Kawase-Koga Y, Zhang S, Visvader J, Toth M, Walsh CA, Sun T (2009) Transcription
845 factor Lmo4 defines the shape of functional areas in developing cortices and regulates
846 sensorimotor control. Dev Biol 327:132-142.
847 Hynd GW, Semrud-Clikeman M, Lorys AR, Novey ES, Eliopulos D, Lyytinen H (1991) Corpus
848 callosum morphology in attention deficit-hyperactivity disorder: morphometric analysis
849 of MRI. J Learn Disabil 24:141-146.
850 Innocenti GM, Ansermet F, Parnas J (2003) Schizophrenia, neurodevelopment and corpus
851 callosum. Mol Psychiatry 8:261-274.
852 Innocenti GM, Price DJ (2005) Exuberance in the development of cortical networks. Nat Rev
853 Neurosci 6:955-965.
854 Jin XL, Guo H, Mao C, Atkins N, Wang H, Avasthi PP, Tu YT, Li Y (2000) Emx1-specific
855 expression of foreign genes using "knock-in" approach. Biochem Biophys Res Commun
856 270:978-982.
857 Joshi PS, Molyneaux BJ, Feng L, Xie X, Macklis JD, Gan L (2008) Bhlhb5 regulates the
858 postmitotic acquisition of area identities in layers II-V of the developing neocortex.
859 Neuron 60:258-272.

860 Kashani AH, Qiu Z, Jurata L, Lee SK, Pfaff S, Goebbels S, Nave KA, Ghosh A (2006) Calcium
861 activation of the LMO4 transcription complex and its role in the patterning of
862 thalamocortical connections. J Neurosci 26:8398-8408.
863 Kishi N, Macklis JD (2004) MECP2 is progressively expressed in post-migratory neurons and is
864 involved in neuronal maturation rather than cell fate decisions. Mol Cell Neurosci
865 27:306-321.
866 Kowalczyk T, Pontious A, Englund C, Daza RA, Bedogni F, Hodge R, Attardo A, Bell C,
867 Huttner WB, Hevner RF (2009) Intermediate neuronal progenitors (basal progenitors)
868 produce pyramidal-projection neurons for all layers of cerebral cortex. Cereb Cortex
869 19:2439-2450.
870 Kranc KR, Bamforth SD, Braganca J, Norbury C, van Lohuizen M, Bhattacharya S (2003)
871 Transcriptional coactivator Cited2 induces Bmi1 and Mel18 and controls fibroblast
872 proliferation via Ink4a/ARF. Mol Cell Biol 23:7658-7666.
873 Kranc KR, Schepers H, Rodrigues NP, Bamforth S, Villadsen E, Ferry H, Bouriez-Jones T,
874 Sigvardsson M, Bhattacharya S, Jacobsen SE, Enver T (2009) Cited2 Is an Essential
875 Regulator of Adult Hematopoietic Stem Cells. Stem Cell 5:659-665.
876 Kriegstein A, Noctor S, Martinez-Cerdeno V (2006) Patterns of neural stem and progenitor cell
877 division may underlie evolutionary cortical expansion. Nat Rev Neurosci 7:883-890.
878 Lee S, Lee B, Joshi K, Pfaff SL, Lee JW, Lee SK (2008) A regulatory network to segregate the
879 identity of neuronal subtypes. Dev Cell 14:877-889.
880 Lomber SG, Payne BR, Rosenquist AC (1994) The spatial relationship between the cerebral
881 cortex and fiber trajectory through the corpus callosum of the cat. Behav Brain Res
882 64:25-35.
883 Lou X, Sun S, Chen W, Zhou Y, Huang Y, Liu X, Shan Y, Wang C (2011) Negative feedback
884 regulation of NF-kappaB action by CITED2 in the nucleus. J Immunol 186:539-548.
885 Luo L, O'Leary DD (2005) Axon retraction and degeneration in development and disease. Annu
886 Rev Neurosci 28:127-156.
887 Macdonald JL, Verster A, Berndt A, Roskams AJ (2010) MBD2 and MeCP2 regulate distinct
888 transitions in the stage-specific differentiation of olfactory receptor neurons. Mol Cell
889 Neurosci 44:55-67.

890 Maguire CA, Bovenberg MS, Crommentuijn MH, Niers JM, Kerami M, Teng J, Sena-Esteves
891 M, Badr CE, Tannous BA (2013) Triple bioluminescence imaging for in vivo monitoring
892 of cellular processes. Mol Ther Nucleic Acids 2:e99.
893 Martinez-Cerdeno V, Noctor SC, Kriegstein AR (2006) The role of intermediate progenitor cells
894 in the evolutionary expansion of the cerebral cortex. Cereb Cortex 16 Suppl 1:i152-161.
895 Michell AC, Braganca J, Broadbent C, Joyce B, Franklyn A, Schneider JE, Bhattacharya S,
896 Bamforth SD (2010) A novel role for transcription factor Lmo4 in thymus development
897 through genetic interaction with Cited2. Dev Dyn 239:1988-1994.
898 Mitchell BD, Macklis JD (2005) Large-scale maintenance of dual projections by callosal and
899 frontal cortical projection neurons in adult mice. J Comp Neurol 482:17-32.
900 Miyata T, Kawaguchi A, Saito K, Kawano M, Muto T, Ogawa M (2004) Asymmetric production
901 of surface-dividing and non-surface-dividing cortical progenitor cells. Development
902 131:3133-3145.
903 Mizuno H, Hirano T, Tagawa Y (2007) Evidence for activity-dependent cortical wiring:
904 formation of interhemispheric connections in neonatal mouse visual cortex requires
905 projection neuron activity. J Neurosci 27:6760-6770.
906 Molnar Z, Metin C, Stoykova A, Tarabykin V, Price DJ, Francis F, Meyer G, Dehay C, Kennedy
907 H (2006) Comparative aspects of cerebral cortical development. Eur J Neurosci 23:921-
908 934.
909 Molyneaux BJ, Arlotta P, Fame RM, MacDonald JL, MacQuarrie KL, Macklis JD (2009) Novel
910 Subtype-specific Genes Identify Distinct Subpopulations of Callosal Projection Neurons.
911 J Neurosci 29.
912 Motulsky HJ, Brown RE (2006) Detecting outliers when fitting data with nonlinear regression - a
913 new method based on robust nonlinear regression and the false discovery rate. BMC
914 Bioinformatics 7:123.
915 Mukaetova-Ladinska EB, Arnold H, Jaros E, Perry R, Perry E (2004) Depletion of MAP2
916 expression and laminar cytoarchitectonic changes in dorsolateral prefrontal cortex in
917 adult autistic individuals. Neuropathol Appl Neurobiol 30:615-623.
918 Noctor SC, Martinez-Cerdeno V, Ivic L, Kriegstein AR (2004) Cortical neurons arise in
919 symmetric and asymmetric division zones and migrate through specific phases. Nat
920 Neurosci 7:136-144.

921 Noctor SC, Martínez-Cerdeño V, Kriegstein AR (2008) Distinct behaviors of neural stem and
922 progenitor cells underlie cortical neurogenesis. J Comp Neurol 508:28-44.
923 O'Leary DD, Chou SJ, Sahara S (2007) Area patterning of the mammalian cortex. Neuron
924 56:252-269.
925 Olivares R, Montiel J, Aboitiz F (2001) Species differences and similarities in the fine structure
926 of the mammalian corpus callosum. Brain Behav Evol 57:98-105.
927 Paul LK, Brown WS, Adolphs R, Tyszka JM, Richards LJ, Mukherjee P, Sherr EH (2007)
928 Agenesis of the corpus callosum: genetic, developmental and functional aspects of
929 connectivity. Nat Rev Neurosci 8:287-299.
930 Pinto L, Drechsel D, Schmid M-T, Ninkovic J, Irmler M, Brill MS, Restani L, Gianfranceschi L,
931 Cerri C, Weber SN, Tarabykin V, Baer K, Guillemot F, Beckers J, Zecevic N, Dehay C,
932 Caleo M, Schorle H, Götz M (2009) AP2γ regulates basal progenitor fate in a region- and
933 layer-specific manner in the developing cortex. Nat Neurosci 12:1229-1237.
934 Piven J, Bailey J, Ranson BJ, Arndt S (1997) An MRI study of the corpus callosum in autism.
935 Am J Psychiatry 154:1051-1056.
936 Plessen KJ, Gruner R, Lundervold A, Hirsch JG, Xu D, Bansal R, Hammar A, Lundervold AJ,
937 Wentzel-Larsen T, Lie SA, Gass A, Peterson BS, Hugdahl K (2006) Reduced white
938 matter connectivity in the corpus callosum of children with Tourette syndrome. J Child
939 Psychol Psychiatry 47:1013-1022.
940 Polleux F, Dehay C, Goffinet A, Kennedy H (2001) Pre- and post-mitotic events contribute to
941 the progressive acquisition of area-specific connectional fate in the neocortex. Cereb
942 Cortex 11:1027-1039.
943 Pontious A, Kowalczyk T, Englund C, Hevner RF (2008) Role of intermediate progenitor cells
944 in cerebral cortex development. Dev Neurosci 30:24-32.
945 Preis JI, Wise N, Solloway MJ, Harvey RP, Sparrow DB, Dunwoodie SL (2006) Generation of
946 conditional Cited2 null alleles. Genesis 44:579-583.
947 Rash BG, Grove EA (2006) Area and layer patterning in the developing cerebral cortex. Curr
948 Opin Neurobiol 16:25-34.
949 Roessner V, Banaschewski T, Uebel H, Becker A, Rothenberger A (2004) Neuronal network
950 models of ADHD -- lateralization with respect to interhemispheric connectivity
951 reconsidered. Eur Child Adolesc Psychiatry 13 Suppl 1:I71-79.

952 Rosen GD, Azoulay NG, Griffin EG, Newbury A, Koganti L, Fujisaki N, Takahashi E, Grant
953 PE, Truong DT, Fitch RH, Lu L, Williams RW (2013) Bilateral subcortical heterotopia
954 with partial callosal agenesis in a mouse mutant. Cereb Cortex 23:859-872.
955 Schuurmans C, Armant O, Nieto M, Stenman JM, Britz O, Klenin N, Brown C, Langevin LM,
956 Seibt J, Tang H, Cunningham JM, Dyck R, Walsh C, Campbell K, Polleux F, Guillemot
957 F (2004) Sequential phases of cortical specification involve Neurogenin-dependent and -
958 independent pathways. Embo J 23:2892-2902.
959 Seidman LJ, Valera EM, Makris N (2005) Structural brain imaging of attention-
960 deficit/hyperactivity disorder. Biol Psychiatry 57:1263-1272.
961 Sessa A, Mao CA, Hadjantonakis AK, Klein WH, Broccoli V (2008) Tbr2 directs conversion of
962 radial glia into basal precursors and guides neuronal amplification by indirect
963 neurogenesis in the developing neocortex. Neuron 60:56-69.
964 Shetty RS, Bose SC, Nickell MD, McIntyre JC, Hardin DH, Harris AM, McClintock TS (2005)
965 Transcriptional changes during neuronal death and replacement in the olfactory
966 epithelium. Mol Cell Neurosci 30:583-600.
967 Sholl DA (1953) Dendritic organization in the neurons of the visual and motor cortices of the
968 cat. J Anat 87:387-406.
969 Song JW, Mitchell PD, Kolasinski J, Ellen Grant P, Galaburda AM, Takahashi E (2015)
970 Asymmetry of White Matter Pathways in Developing Human Brains. Cereb Cortex
971 25:2883-2893.
972 Srivastava DP, Woolfrey KM, Jones KA, Anderson CT, Smith KR, Russell TA, Lee H,
973 Yasvoina MV, Wokosin DL, Ozdinler PH, Shepherd GM, Penzes P (2012) An autism-
974 associated variant of Epac2 reveals a role for Ras/Epac2 signaling in controlling basal
975 dendrite maintenance in mice. PLoS Biol 10:e1001350.
976 Suarez R, Fenlon LR, Marek R, Avitan L, Sah P, Goodhill GJ, Richards LJ (2014) Balanced
977 interhemispheric cortical activity is required for correct targeting of the corpus callosum.
978 Neuron 82:1289-1298.
979 Swayze VW, 2nd, Andreasen NC, Ehrhardt JC, Yuh WT, Alliger RJ, Cohen GA (1990)
980 Developmental abnormalities of the corpus callosum in schizophrenia. Arch Neurol
981 47:805-808.

Takahashi E, Dai G, Wang R, Ohki K, Rosen GD, Galaburda AM, Grant PE, Wedeen VJ (2010) Development of cerebral fiber pathways in cats revealed by diffusion spectrum imaging. NeuroImage 49:1231-1240.

Tibbo P, Nopoulos P, Arndt S, Andreasen NC (1998) Corpus callosum shape and size in male patients with schizophrenia. Biol Psychiatry 44:405-412.

Tuch DS, Reese TG, Wiegell MR, Wedeen VJ (2003) Diffusion MRI of complex neural architecture. Neuron 40:885-895.

Tuoc TC, Narayanan R, Stoykova A (2013) BAF chromatin remodeling complex: cortical size regulation and beyond. Cell Cycle 12:2953-2959.

Wang C, Zhang L, Zhou Y, Zhou J, Yang X, Duan S, Xiong Z, Ding Y (2007) Activity-Dependent Development of Callosal Projections in the Somatosensory Cortex. Journal of Neuroscience 27:11334-11342.

Weninger WJ, Lopes Floro K, Bennett MB, Withington SL, Preis JI, Barbera JP, Mohun TJ, Dunwoodie SL (2005) Cited2 is required both for heart morphogenesis and establishment of the left-right axis in mouse development. Development 132:1337-1348.

Wilson CJ (1987) Morphology and synaptic connections of crossed corticostriatal neurons in the rat. J Comp Neurol 263:567-580.

Withington SL, Scott AN, Saunders DN, Lopes Floro K, Preis JI, Michalicek J, Maclean K, Sparrow DB, Barbera JP, Dunwoodie SL (2006) Loss of Cited2 affects trophoblast formation and vascularization of the mouse placenta. Dev Biol 294:67-82.

Wolf RC, Hose A, Frasch K, Walter H, Vasic N (2008) Volumetric abnormalities associated with cognitive deficits in patients with schizophrenia. Eur Psychiatry 23:541-548.

Xu B, Qu X, Gu S, Doughman YQ, Watanabe M, Dunwoodie SL, Yang YC (2008) Cited2 is required for fetal lung maturation. Dev Biol 317:95-105.

Zhou J, Wen Y, She L, Sui YN, Liu L, Richards LJ, Poo MM (2013) Axon position within the corpus callosum determines contralateral cortical projection. Proc Natl Acad Sci U S A 110:E2714-2723.

Figure Legends:

Figure 1: *Cited2* is expressed broadly by CPN progenitors at E15.5, with expression refining to CPN of somatosensory cortex by P3

(A) *Cited2* is highly expressed by callosal projection neurons (CPN; red) relative to corticospinal motor neurons (CSMN; blue) at critical times during development, as detected by microarray analysis of FACS-purified CPN and CSMN. Error bars denote SEM (Molyneaux et al., 2009). (B) Western blot analysis showing that CITED2 protein is highly expressed as early as E15.5 in the neocortex, with expression decreasing postnatally, relative to a β-actin loading control. (C) Expression of *Cited2* is largely restricted to subpallial progenitors at E13.5, but (D) *Cited2* is highly expressed in the cortical subventricular zone (SVZ) at E15.5, the peak of superficial layer CPN birth, with (E-F) expression maintained in layers II/III, and V postnatally. (G) Embryonically, *Cited2* is expressed uniformly across the neocortex, detected across the SVZ at E18.5 (arrowheads), and across the cortical plate (CP). (H) In the first days postnatally, however, its expression refines and becomes restricted to somatosensory cortex (arrows) by P3. (I) At E15.5, *Cited2* is highly expressed in the subventricular zone (SVZ), extending into the intermediate zone (IZ). (J) *Cited2* (blue) is largely excluded from PAX6+ (green) radial glial progenitors of the ventricular zone (VZ), but is highly expressed by TBR2+ (red) intermediate progenitor cells (IPCs) of the SVZ. (K) *Cited2* is largely excluded from the highly proliferative, Ki67+ (green) VZ and apical mitotic cells, as indicated by pH3 (red), but is expressed by basally-proliferating IPCs of the SVZ and IZ, VZ = ventricular zone; SVZ = subventricular zone; IZ = intermediate zone; CP = cortical plate. Scale bars in (C-F) = 500μm; (G, H, I) = 1mm (C',-H', J-K) = 100μm; (I')=200μm. Dotted lines in J and K indicate apical, ventricular surface.

Figure 2: Loss of *Cited2* function results in specific reduction of TBR2+ IPCs in E15.5 neocortex

(A-A") At E15.5, the peak of *Cited2* expression, there is no change in the overall number of (PAX6+) radial glial progenitors in *Cited2*;*Emx1-Cre* conditional knockout neocortex (cKO) compared to control littermates (WT). (B-B'') There is, however, a significant reduction in the number of TBR2+ intermediate progenitor cells (IPCs), which largely give rise to superficial layer CPN at this stage of development. Reduction in TBR2+ IPCs might result from (C-C'') reduced proliferation of IPCs, as indicated by proliferating cell nuclear antigen (PCNA, red) and TBR2 (green) double positivity (N = 11 WT, 6 cKO for A-C); (D-D'') specific reduction in basal cell divisions, as indicated by position of pH3-positive mitotic cells (N = 10 WT, 5 cKO); and/or (E) increased cell death, as indicated by expression of activated caspase-3+ (aC3). There is increased apoptotic cell death in *Cited2* cKO neocortex, both within the progenitor population and post-mitotically (N = 11 WT, 6 cKO). (F-F'') To directly investigate whether *Cited2* cell-autonomously regulates proliferation of IPCs, we electroporated Cre recombinase and GFP into VZ progenitors of $Cited2^{fl/fl}$ and $Cited2^{fl/wt}$ littermates at E14.5, to excise *Cited2* in a small subpopulation of neocortical progenitors. We employed a BrdU pulse at E15.5, and immunocytochemistry for Ki67 at E16.5 to identify progenitors that continued to proliferate. There is a significant reduction in the number of *Cited2*-null ($Cited2^{fl/fl}$; Cre+) progenitors that incorporate BrdU at E15.5, or express Ki67+ at E16.5, demonstrating that *Cited2*-null IPCs are less likely to re-enter the cell cycle than their heterozygous counterparts. There is no change in the number of aC3+ cells in the *Cited2*-null progenitors at E16.5. (N = 4 $Cited2^{fl/wt}$; 5 $Cited2^{fl/fl}$). Scale bars = 100μm. Error bars denote SEM. * $p<0.05$; ** $p<0.001$ (Student's t-test)

Figure 3: Loss of *Cited2* function results in reduced superficial layer thickness and total neocortical length at P3

(A) At P6, *Cited2* cKO neocortex is smaller than in WT littermate controls, but both CPN (SATB2+) and CSMN (CTIP2+) are present and appropriately positioned. (B) Anterograde labeling with DiI and (C) retrograde labeling with CTB demonstrate that CPN are present and are targeting the contralateral hemisphere in *Cited2* cKO neocortex. However, both the distribution of retrogradely-labeled CPN (C), and (D) CUX1 (red, superficial layers) and CTIP2 (green, deep layers) immunocytochemistry, indicate that superficial layers are reduced in thickness in the *Cited2* cKO neocortex, while deep layers are not changed in thickness (N = 4-5 per genotype for A-D). (E) Quantitative analysis of neocortical layer thickness at P3 reveals that superficial layers (II-IV; LMO4, red) are significantly reduced in thickness in motor, somatosensory, and visual neocortical areas of P3 *Cited2* cKO, in comparison to control littermates. There is no change in deep layer thickness (V-VI; CTIP2, green) in any region (N = 8 WT, 4 cKO). (F) *Cited2* cKO cortex is visibly smaller than in control littermates at P3, both in wholemount view and in sagittal sections. (G) There is a significant reduction in total neocortical surface rostrocaudal length of approximately 10%, as measured on four sagittal sections across the medio-lateral axis (N = 8 WT, 4 cKO). Scale bar in A = 1mm, B = 50μm. Error bars denote SEM. * $p < 0.05$; ** $p < 0.001$ (Student's t-test)

Figure 4: Neocortical surface length reduction is restricted to layers II/III of somatosensory cortex in P3 *Cited2* cKO neocortex

(A-C) Analysis of three broad neocortical areas identified by LMO4 expression at P3 indicates a highly specific and substantial reduction (~30%) in rostro-caudal surface length of the somatosensory

area (blue) in *Cited2* cKO neocortex, entirely accounting for the total cortical surface length reduction (N = 8 WT, 4 cKO). (D-G) Reduced somatosensory cortex length (black arrowheads) was confirmed via expression of multiple genes either excluded from superficial layers of somatosensory cortex (D,E; *Cadh8, EphA7*), or specifically expressed in somatosensory cortex (F; *ephrinA5*). Measurements of acallosal layer IV somatosensory cortex (black arrows), in contrast (F,G; *ephrinA5, Rorβ*), reveals that there is no significant difference in non-CPN somatosensory cortex length in *Cited2* cKO compared to WT (N = 8 WT, 4 cKO). (H-H''') In P3 *Cited2* WT neocortex, molecular markers of layer IV (green, RORβ; bracket) and somatosensory cortex in layers II/III (red, Bhlhb5; white line) align at the motor / somatosensory border, shown in sagittal view (rostral to left). (I-I''') In P3 *Cited2* cKO neocortex, in contrast, the boundary of layer II/III expression of Bhlhb5 (white line, with additional low-level expression indicated by dashed line) is located caudal to layer IV RORβ expression (bracket), resulting in a misalignment of molecular areal boundaries between CPN of layer II/III and acallosal layer IV (schematized in H''' and I''') (N = 4-5 per genotype). Scale bar in D-G = 500μm, H-I = 200μm. Error bars denote SEM. * $p < 0.05$; ** $p < 0.001$ (Student's t-test)

Figure 5: Additional loss of *Lmo4* function does not alter *Cited2* cKO neocortical thickness, but does reestablish layer II/III somatosensory neocortical length at the expense of motor cortex.

(A-C) Additional loss of *Lmo4* function in *Cited2* null neocortex ($Cited2^{fl/fl};Lmo4^{fl/fl};Emx1^{Cre/+}$) does not alter the reduced reduction in superficial layer thickness of *Cited2* null motor or visual cortex, but does increase superficial layer thickness in somatosensory cortex. Additional loss of *Lmo4* function does not alter the overall reduction in total neocortical length (data not shown). (D-G) Additional loss of *Lmo4* function does, however, reestablish layer II/III somatosensory neocortical length (as measured by Bhlhb5 expression) to normal control length, at the expense

of layer II/III motor cortex. (H) Length of motor (rostral to Bhlhb5 layer II/III expression), somatosensory (Bhlhb5 layer II/III positive), and visual (caudal to layer II/III Bhlhb5 expression) cortical areas was measured in control (*Emx1-cre* negative), *Lmo4* cKO (*Cited2*$^{+/+}$;*Lmo4*$^{fl/fl}$;*Emx1*$^{Cre/+}$), *Cited2* cKO (*Cited2*$^{fl/fl}$;*Lmo4*$^{+/+}$;*Emx1*$^{Cre/+}$), and double cKO (*Cited2*$^{fl/fl}$;*Lmo4*$^{fl/fl}$;*Emx1*$^{Cre/+}$) littermates. (I-L) In the context of the shortened neocortical surface length in *Cited2* cKO mice, additional loss of *Lmo4* function reestablishes the length of the somatosensory area boundary, at the expense of motor cortex length. Loss of *Lmo4* function has no effect on the overall reduced neocortical length or layer II/III thickness of *Cited2* cKO neocortex, in contrast. Scale bars in (C) = 100μm; (D-G) 1mm. For each neocortical area, data were analyzed by a one-way ANOVA with Tukey post-test. For all experiments, N = 14 controls, 7 *Lmo4* cKO, 7 *Cited2* cKO, and 8 double cKO. Error bars denote SEM. * $p < 0.05$, **$p < 0.001$, ***$p < 0.0001$.

Figure 6: Excision of *Cited2* post-mitotically via *NEX-Cre* does not alter neocortical laminar thickness or neocortical area lengths.

(A) *NEX-Cre* mediated post-mitotic excision of *Cited2* does not visibly alter brain morphology or neocortical laminar development at P6 (as indicated by DAPI nuclear staining), and (B) there is no significant difference in P3 neocortical length between *Cited2*; *NEX-Cre* cKO mice and control littermates. Further, (C-C'') there is no change in the overall neocortical laminar thickness of superficial or deep layers in P3 *Cited2*; *NEX-cre* cKO neocortex, nor (D-E) is there a change in the length of motor, somatosensory, or visual neocortical area lengths in *Cited2*; NEX-*Cre* cKO neocortex. For all experiments, N = 4 WT, 4 cKO. Scale bar in A = 1 mm, C = 100 μm. Error bars denote SEM.

Figure 7: Loss of *Cited2* function results in aberrant dendritic complexity of superficial layer somatosensory CPN

(A-A') Neuronal soma size (NeuN area) is not affected by loss of *Cited2*. Increased neuronal density is evident here, consistent with the modest, but significant, increase in cell density in layer II/III of somatosensory cortex (23% increase, p=0.01) quantified at P6 (see Results text). N = 3 WT, 3 cKO. (B-D) Dendritic complexity of layer II/III pyramidal neurons (primarily CPN) was analyzed at P22 by Golgi staining and Sholl analysis in *Cited2;Emx1-cre* cKO neocortex, in comparison to control littermates. There is no significant difference in dendritic complexity of layer II/III CPN in (B-B') motor cortex or (D-D') visual cortex of *Cited2; Emx1-cre* cKO mice, compared to littermate controls. (C-C') There is, however, a significant increase in dendritic complexity of layer II/III CPN in somatosensory cortex of *Cited2;Emx1-cre* cKO (two-way ANOVA $p < 0.0001$). (E) CPN of motor cortex are more complex than CPN of somatosensory or visual cortex (two-way ANOVA $p < 0.0001$). (F) In *Cited2; Emx1-Cre* cKO mice, dendritic complexity of somatosensory CPN is not significantly different from CPN of motor cortex (two-way ANOVA $p = 0.16$), suggesting that somatosensory CPN might be partially "motorized" in the absence of *Cited2* function. (G-I) Dendritic complexity of layer II/III CPN was analyzed at P22 by Golgi staining and Sholl analysis in *Cited2*;*NEX-Cre* conditional knockout neocortex, in comparison to control littermates. Following this post-mitotic loss of *Cited2* function, there is no change in dendritic complexity of superficial layer pyramidal neurons in any of the primary areas examined (motor, somatosensory, or visual). Scale bars = 50µm. * $p < 0.05$, ** $p < 0.01$, *** $p < 0.001$, Bonferroni post-test in B, C, D, E, F, G). (B-E) Motor: N = 17 WT, 12 cKO; Somatosensory: N = 27 WT, 14 cKO; Visual: N = 18 WT, 9

cKO. (G-I) Motor: N = 38 WT, 34 cKO; Somatosensory: N = 37 WT, 20 cKO; Visual: N = 34 WT, 19 cKO.

Figure 8: Interhemispheric CPN axonal connectivity is disrupted in adult *Cited2* cKO neocortex

(A-B) HARDI tractography analysis of interhemispheric connections demonstrates a significant reduction in the size of the corpus callosum (CC), and in the number of callosal fibers in juvenile/ young adult (9wks) *Cited2; Emx1 cre* cKO neocortex, compared to littermate controls, particularly within the mid-CC (corresponding to somatosensory cortex). Reconstructed pathways are superimposed on the mean diffusion-weighted magnetic resonance image of the brain. Pathways running between right and left are red; dorsal and ventral are green; and anterior and posterior are blue. The images do not include anterior commissure or olfactory bulb fibers; these were removed a priori to focus on the CC. Images in A' and B' similarly exclude hippocampal commissure fibers. N = 2 WT, 2 cKO. (C-D) Staining for myelin basic protein in sagittal sections of *Cited2* WT and cKO brains followed by measurement of midsagittal CC area (D) identifies a reduction in CC area in *Cited2* cKO brains, but demonstrates the structural integrity of the CC throughout all areas. N = 3 WT, 4 cKO. (E-K) To investigate precision of callosal projections in the absence of *Cited2* function, a focal injection of the anterograde tracer AAV-GFP was made in somatosensory (extending into motor) neocortex at P6, and contralateral callosal projections were analyzed at 6 weeks of age. In contrast to the precise homotopic projections observed in *Cited2* WTs (G), callosal projections in *Cited2* cKO somatosensory neocortex are diffuse (J). (K) Relative GFP fluorescence intensity was measured in matched sagittal sections of the left, injected neocortical hemisphere, and in the same region in the

contralateral, projection hemisphere, demonstrating consistent caudal spread of callosal projections in *Cited2* cKO neocortex. N = 3 WT, 3 cKO. ANOVA analysis finds no change in the anterior tail (-1400µm to -800µm) or center (-700µm to 700µm) regions, but the posterior tail (800µm to 1400µm) of the cKO distribution is significantly different than that of the WT ($p < 0.0001$). Error bars denote SEM. * $p < 0.05$, (Student's t-test) in C. * $p < 0.001$ (Bonferroni-post test) in K. Scale bar in A-B = 1.5mm, C,D, F,G, I,J = 1mm, G',J' = 500µm.

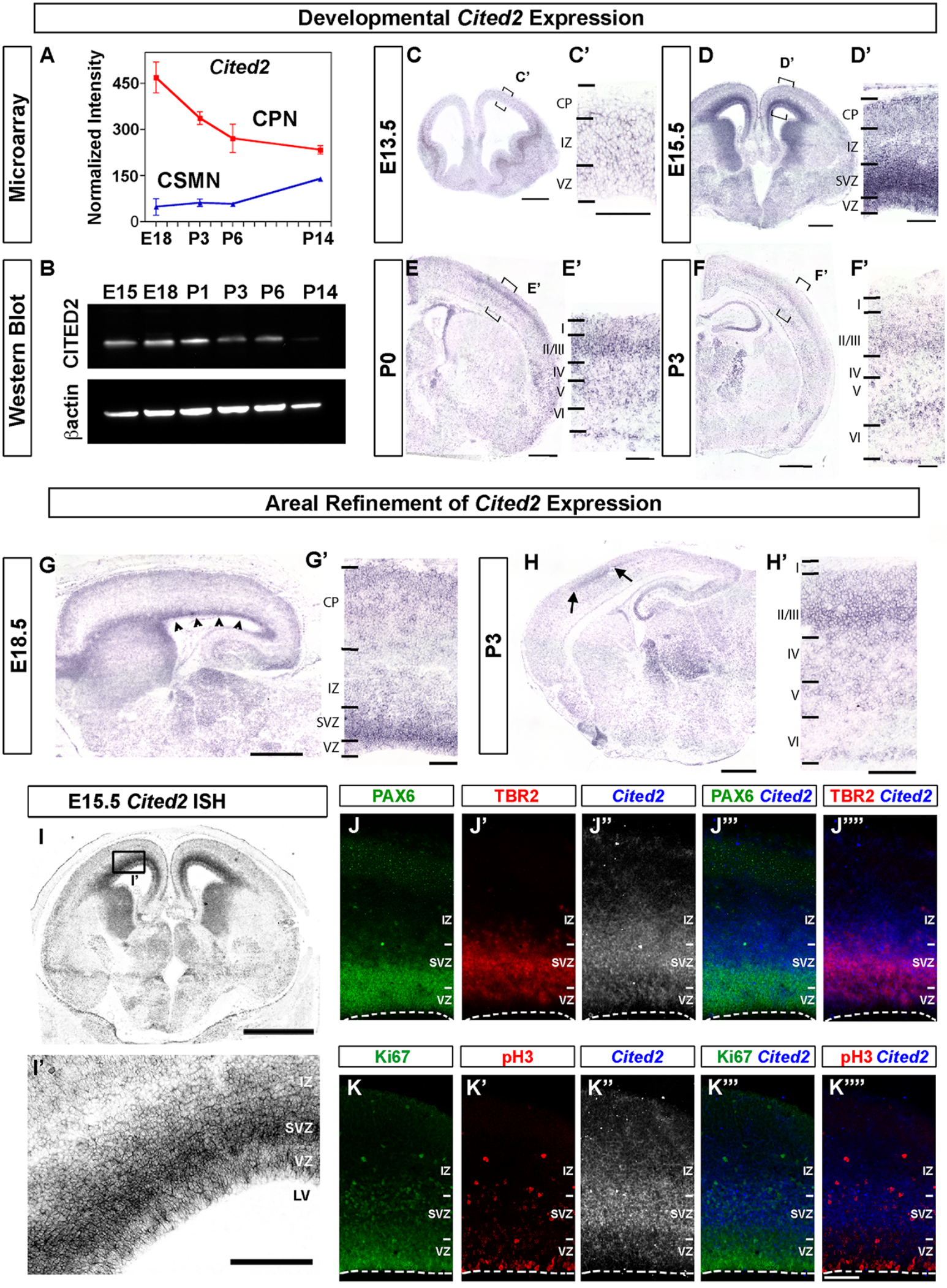
Developmental Cited2 Expression
Microarray
A
Cited2
CPN
CSMN
Normalized Intensity
450
300
150
0
E18
P3
P6
P14
Western Blot
B
E15 E18 P1 P3 P6 P14
CITED2
βactin
E13.5
C
C'
CP
IZ
VZ
E15.5
D
D'
CP
IZ
SVZ
VZ
P0
E
E'
I
II/III
IV
V
VI
P3
F
F'
I
II/III
IV
V
VI
Areal Refinement of Cited2 Expression
E18.5
G
G'
CP
IZ
SVZ
VZ
P3
H
H'
I
II/III
IV
V
VI
E15.5 Cited2 ISH
I
I'
IZ
SVZ
VZ
LV
PAX6
TBR2
Cited2
PAX6 Cited2
TBR2 Cited2
J
J'
J''
J'''
J''''
IZ
SVZ
VZ
Ki67
pH3
Cited2
Ki67 Cited2
pH3 Cited2
K
K'
K''
K'''
K''''
IZ
SVZ
VZ

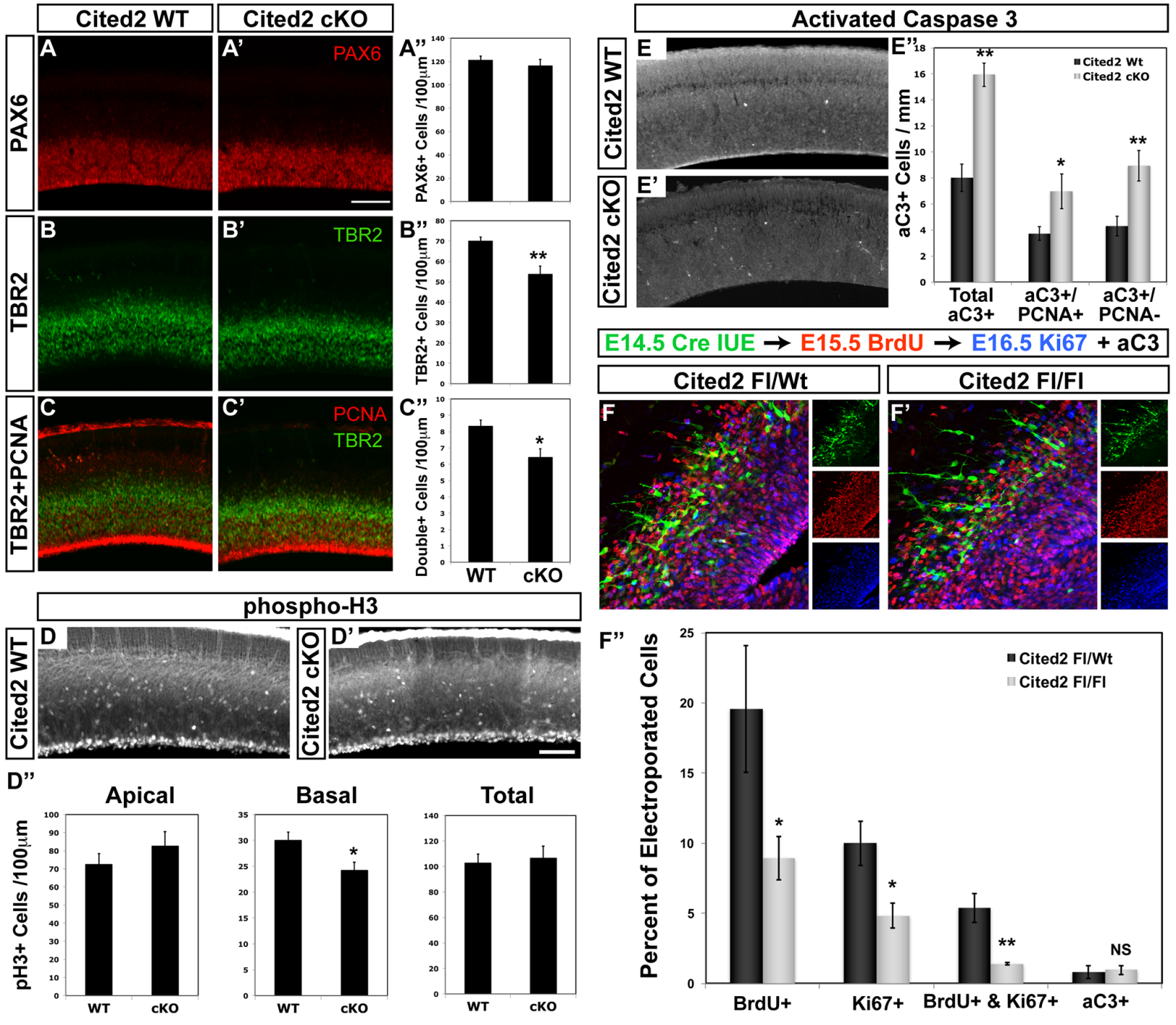
Cited2 WT
Cited2 cKO
PAX6
TBR2
TBR2+PCNA
A
A'
PAX6
A''
PAX6+ Cells /100μm
B
B'
TBR2
B''
TBR2+ Cells /100μm
C
C'
PCNA
TBR2
C''
Double+ Cells /100μm
WT
cKO
Activated Caspase 3
Cited2 WT
Cited2 cKO
E
E'
E''
Cited2 Wt
Cited2 cKO
aC3+ Cells / mm
Total aC3+
aC3+/ PCNA+
aC3+/ PCNA-
E14.5 Cre IUE → E15.5 BrdU → E16.5 Ki67 + aC3
Cited2 Fl/Wt
Cited2 Fl/Fl
F
F'
F''
Percent of Electroporated Cells
BrdU+
Ki67+
BrdU+ & Ki67+
aC3+
NS
phospho-H3
D
D'
D''
Apical
Basal
Total
pH3+ Cells /100μm

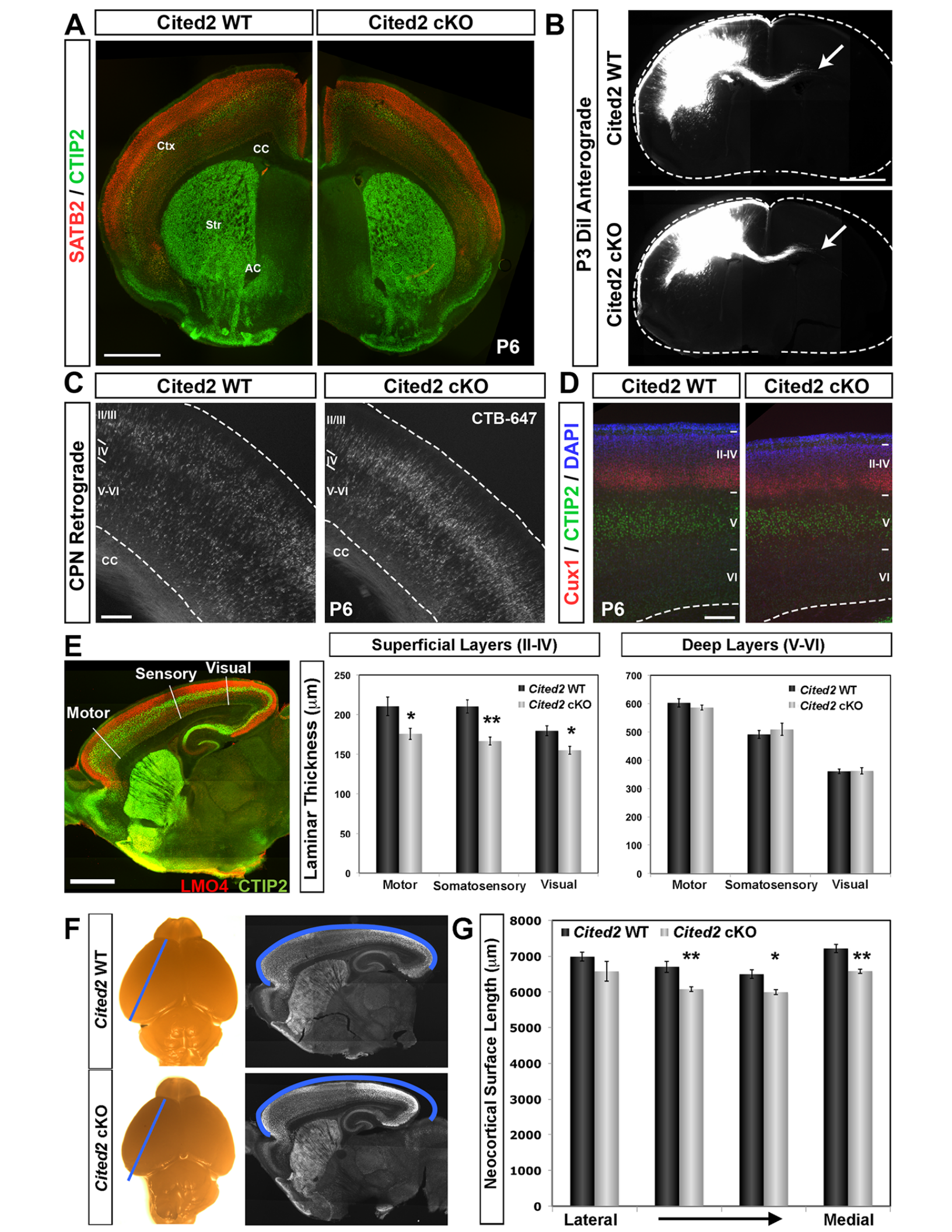
A
Cited2 WT
Cited2 cKO
SATB2 / CTIP2
Ctx
CC
Str
AC
P6
B
P3 DiI Anterograde
Cited2 WT
Cited2 cKO
C
Cited2 WT
Cited2 cKO
CPN Retrograde
II/III
IV
V-VI
CC
CTB-647
P6
D
Cited2 WT
Cited2 cKO
Cux1 / CTIP2 / DAPI
II-IV
V
VI
P6
E
Sensory
Visual
Motor
LMO4 CTIP2
Laminar Thickness (μm)
Superficial Layers (II-IV)
Deep Layers (V-VI)
Cited2 WT
Cited2 cKO
Motor
Somatosensory
Visual
F
Cited2 WT
Cited2 cKO
G
Neocortical Surface Length (μm)
Cited2 WT
Cited2 cKO
Lateral
Medial

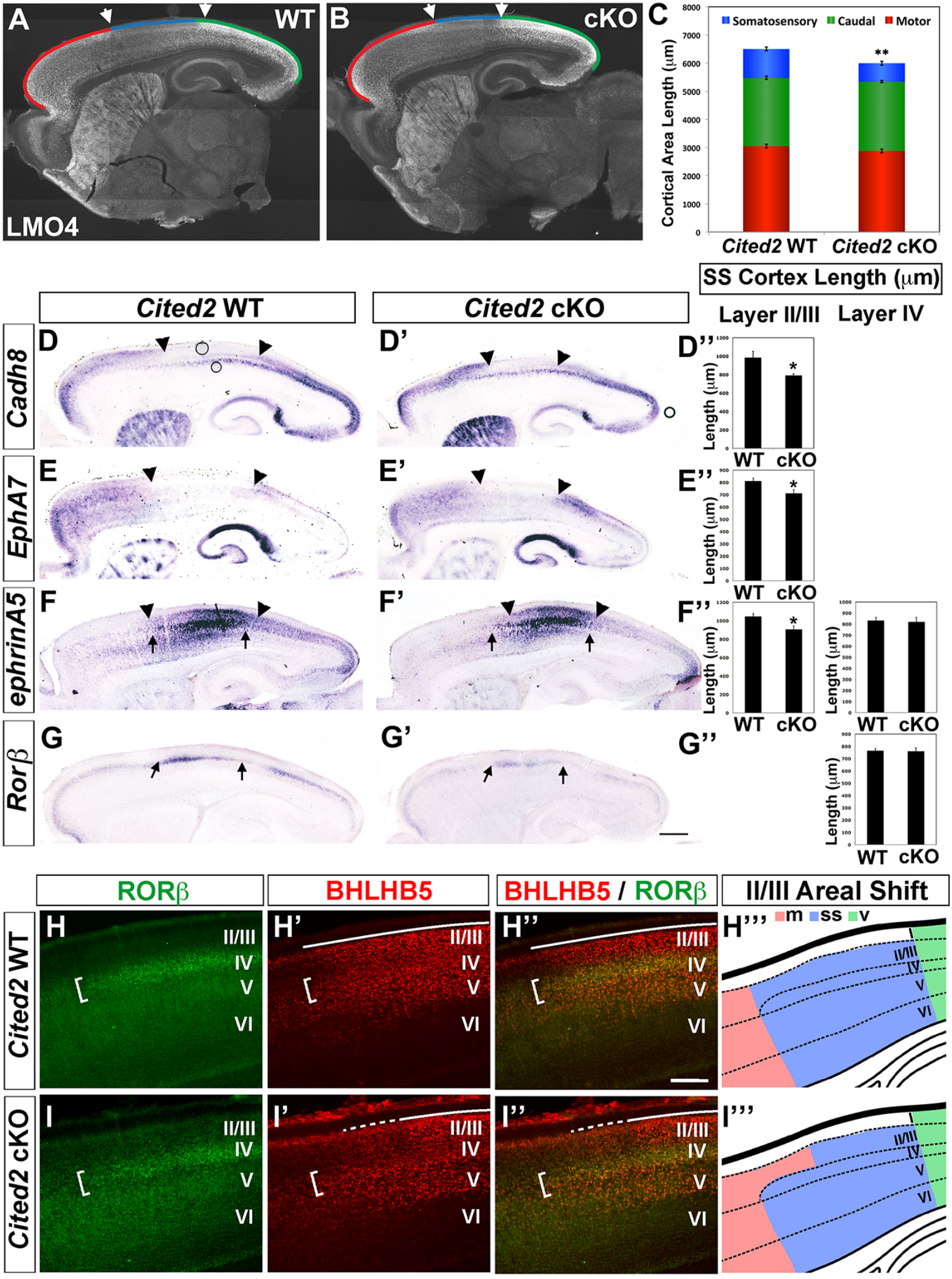
A
WT
LMO4
B
cKO
C
Somatosensory
Caudal
Motor
Cortical Area Length (μm)
8000
7000
6000
5000
4000
3000
2000
1000
0
**
Cited2 WT
Cited2 cKO
SS Cortex Length (μm)
Layer II/III
Layer IV
Cited2 WT
Cited2 cKO
Cadh8
D
D'
D''
EphA7
E
E'
E''
ephrinA5
F
F'
F''
Rorβ
G
G'
G''
Length (μm)
WT
cKO
ROR β
BHLHB5
BHLHB5 / RORβ
II/III Areal Shift
Cited2 WT
Cited2 cKO
H
H'
H''
H'''
I
I'
I''
I'''
II/III
IV
V
VI
m
ss
v

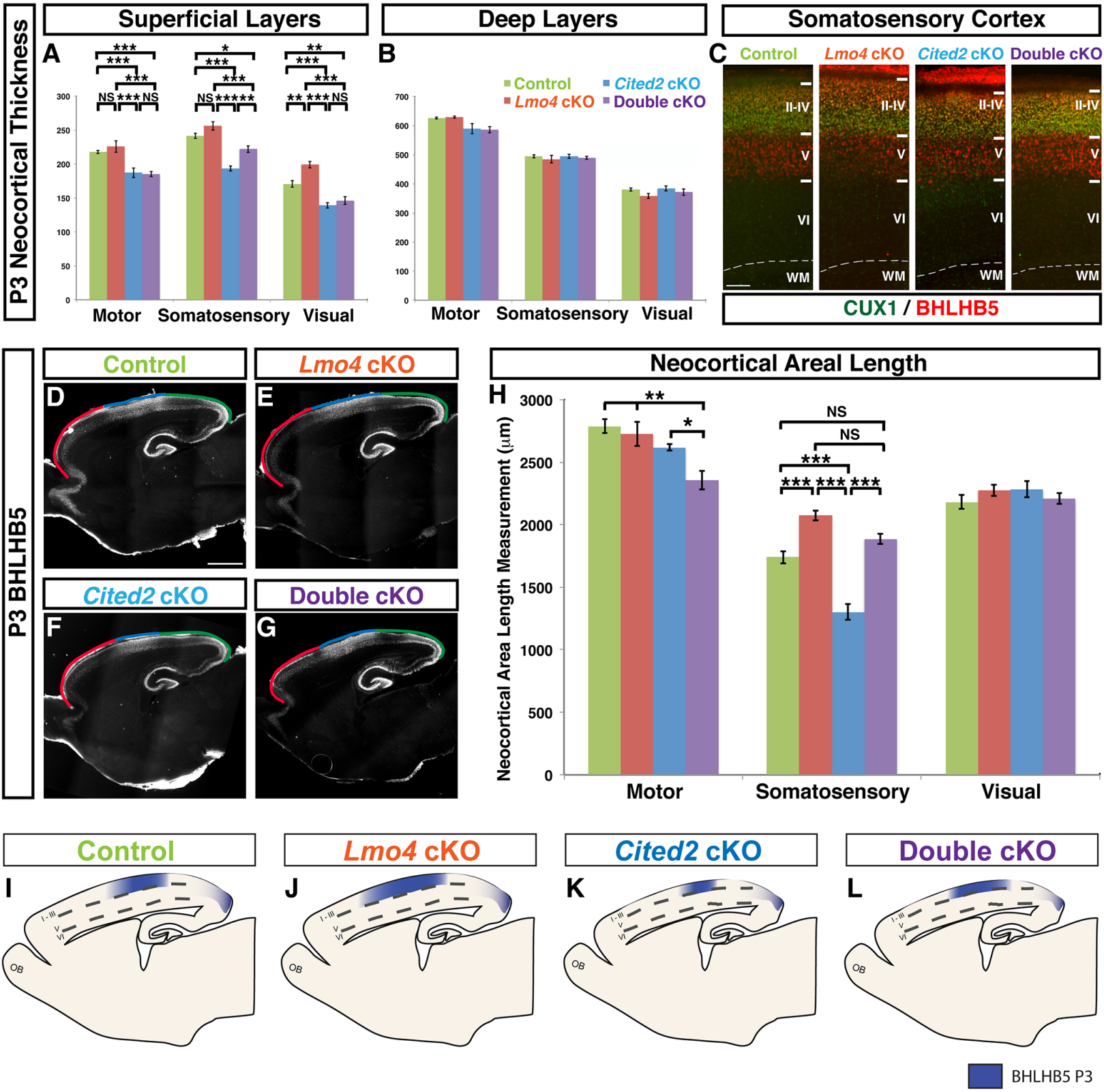
P3 Neocortical Thickness
Superficial Layers
Deep Layers
Somatosensory Cortex
A
B
C
Control
Cited2 cKO
Lmo4 cKO
Double cKO
Motor
Somatosensory
Visual
II-IV
V
VI
WM
CUX1 / BHLHB5
P3 BHLHB5
D
E
F
G
H
Neocortical Areal Length
Neocortical Area Length Measurement (μm)
I
J
K
L
OB
I - III
BHLHB5 P3

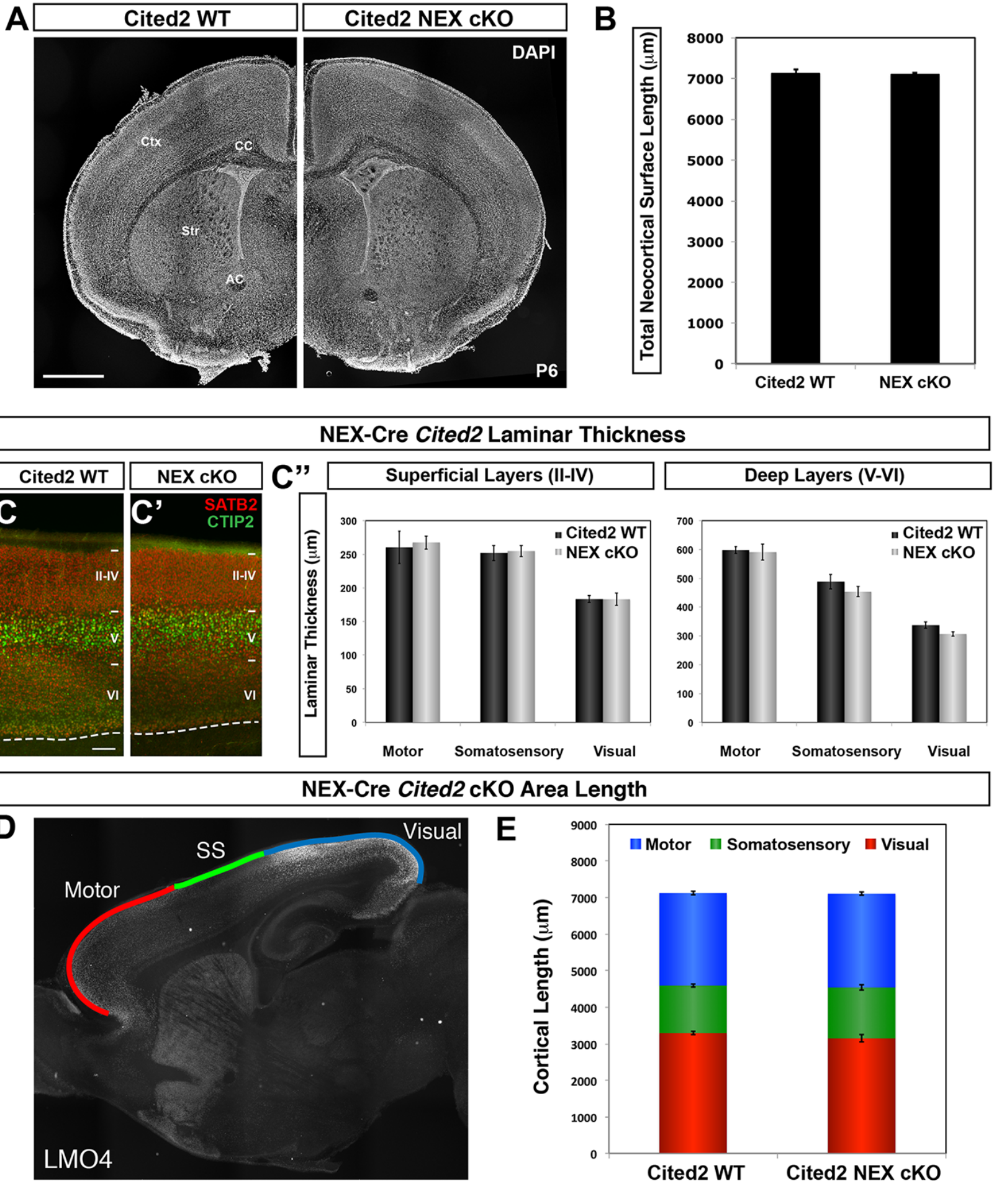
A
Cited2 WT
Cited2 NEX cKO
DAPI
Ctx
CC
Str
AC
P6
B
Total Neocortical Surface Length (μm)
8000
7000
6000
5000
4000
3000
2000
1000
0
Cited2 WT
NEX cKO
NEX-Cre Cited2 Laminar Thickness
Cited2 WT
NEX cKO
C
C'
SATB2
CTIP2
II-IV
V
VI
C''
Superficial Layers (II-IV)
Deep Layers (V-VI)
Laminar Thickness (μm)
300
250
200
150
100
50
0
700
600
500
400
300
200
100
0
Cited2 WT
NEX cKO
Motor
Somatosensory
Visual
NEX-Cre Cited2 cKO Area Length
D
Visual
SS
Motor
LMO4
E
Cortical Length (μm)
9000
8000
7000
6000
5000
4000
3000
2000
1000
0
Motor
Somatosensory
Visual
Cited2 WT
Cited2 NEX cKO

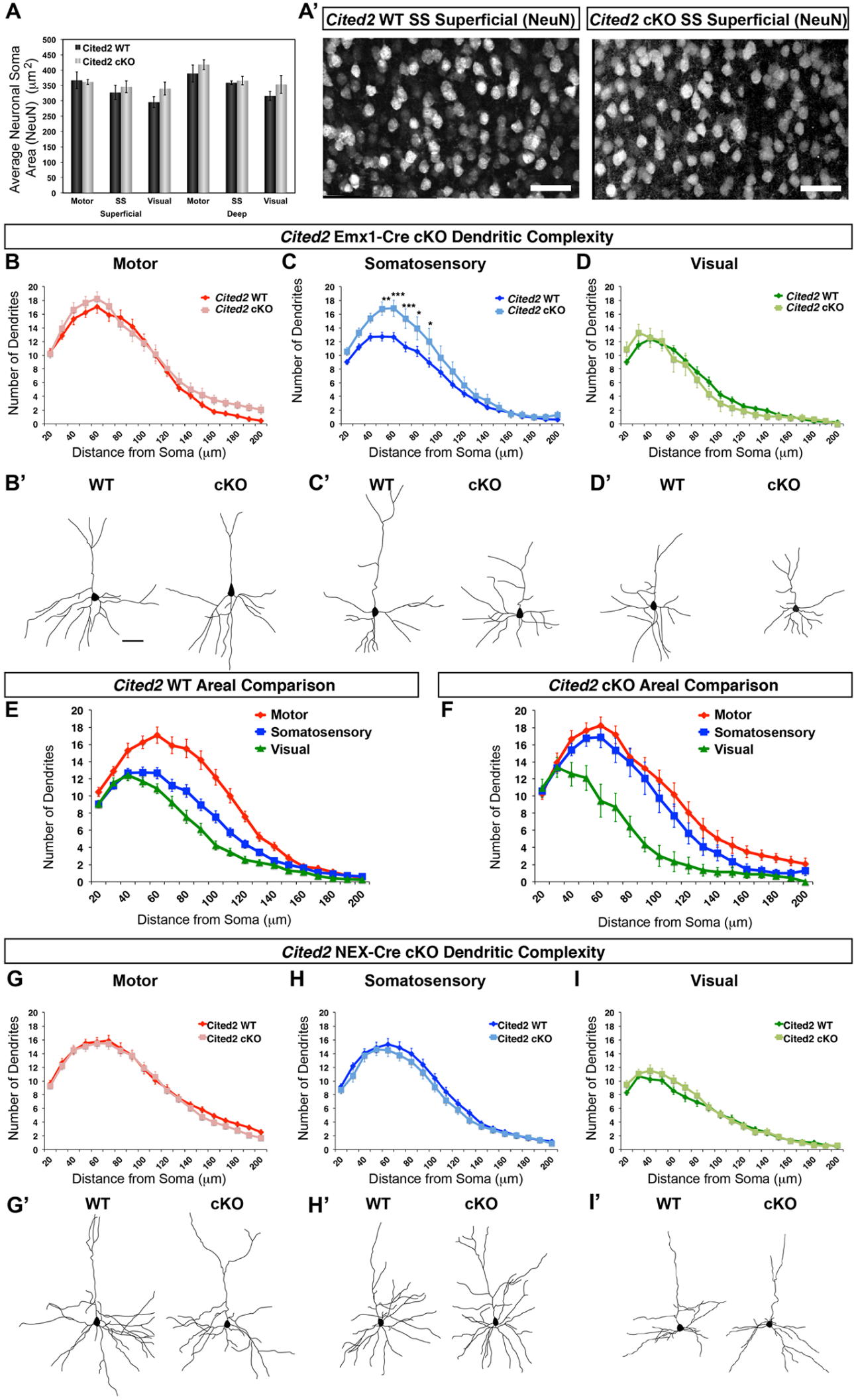
A
Average Neuronal Soma Area (NeuN) (μm²)
Cited2 WT
Cited2 cKO
Motor
SS
Visual
Motor
SS
Visual
Superficial
Deep
A'
Cited2 WT SS Superficial (NeuN)
Cited2 cKO SS Superficial (NeuN)
Cited2 Emx1-Cre cKO Dendritic Complexity
B
Motor
C
Somatosensory
D
Visual
Number of Dendrites
Distance from Soma (μm)
Cited2 WT
Cited2 cKO
B'
WT
cKO
C'
WT
cKO
D'
WT
cKO
Cited2 WT Areal Comparison
Cited2 cKO Areal Comparison
E
F
Motor
Somatosensory
Visual
Cited2 NEX-Cre cKO Dendritic Complexity
G
Motor
H
Somatosensory
I
Visual
G'
WT
cKO
H'
WT
cKO
I'
WT
cKO

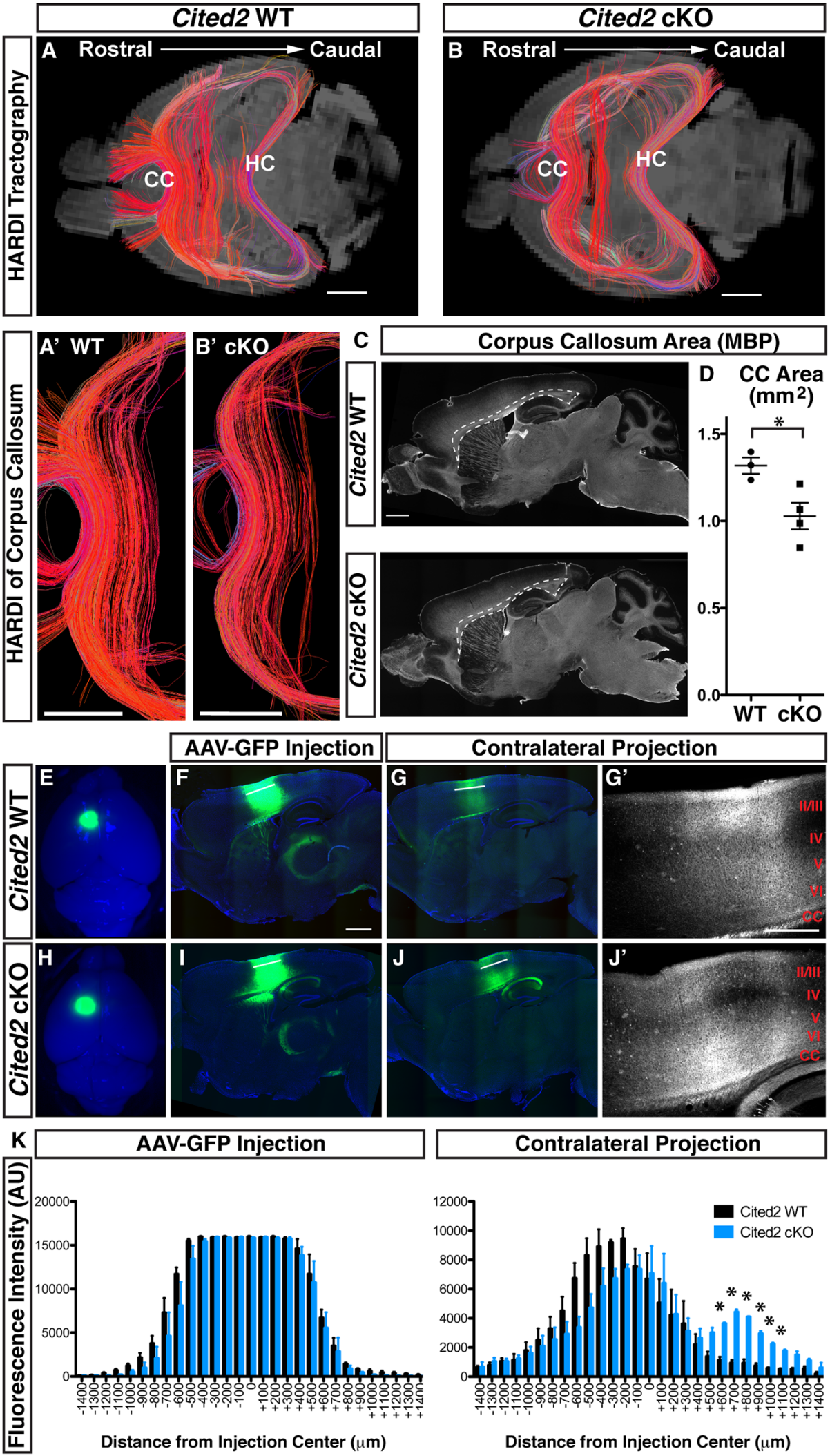
Cited2 WT
Cited2 cKO
HARDI Tractography
A Rostral Caudal
B Rostral Caudal
CC
HC
CC
HC
HARDI of Corpus Callosum
A' WT
B' cKO
C
Corpus Callosum Area (MBP)
Cited2 WT
Cited2 cKO
D CC Area (mm2)
1.5
1.0
0.5
0.0
*
WT cKO
AAV-GFP Injection
Contralateral Projection
E
F
G
G'
H
I
J
J'
II/III
IV
V
VI
CC
K
AAV-GFP Injection
Contralateral Projection
Fluorescence Intensity (AU)
20000
15000
10000
5000
0
12000
10000
8000
6000
4000
2000
Cited2 WT
Cited2 cKO
-1400 -1300 -1200 -1100 -1000 -900 -800 -700 -600 -500 -400 -300 -200 -100 0 +100 +200 +300 +400 +500 +600 +700 +800 +900 +1000 +1100 +1200 +1300 +1400
Distance from Injection Center (μm)
Distance from Injection Center (μm)